

# RoboWheel: A Data Engine from Real-World Human Demonstrations for Cross-Embodiment Robotic Learning

Yuhong Zhang<sup>1,\*</sup> Zihan Gao<sup>1,\*</sup> Shengpeng Li<sup>2</sup> Ling-Hao Chen<sup>1</sup> Kaisheng Liu<sup>2</sup> Runqing Cheng<sup>2</sup>  
 Xiao Lin<sup>2†</sup> Junjia Liu<sup>2,3</sup> Zhuoheng Li<sup>4</sup> Jingyi Feng<sup>5</sup> Ziyuan He<sup>2</sup> Jintian Lin<sup>2</sup>  
 Zheyuan Huang<sup>1</sup> Zhifang Liu<sup>1</sup> Haoqian Wang<sup>1†</sup>

<sup>1</sup>Tsinghua University

<sup>2</sup>Synapath

<sup>3</sup>CUHK

<sup>4</sup>HKU

<sup>5</sup>PolyU

{dsyuhong, gaozihanhu, adreamob, thu.lhchen}@gmail.com

Project page: <https://zhangyuhong01.github.io/Robowheel>

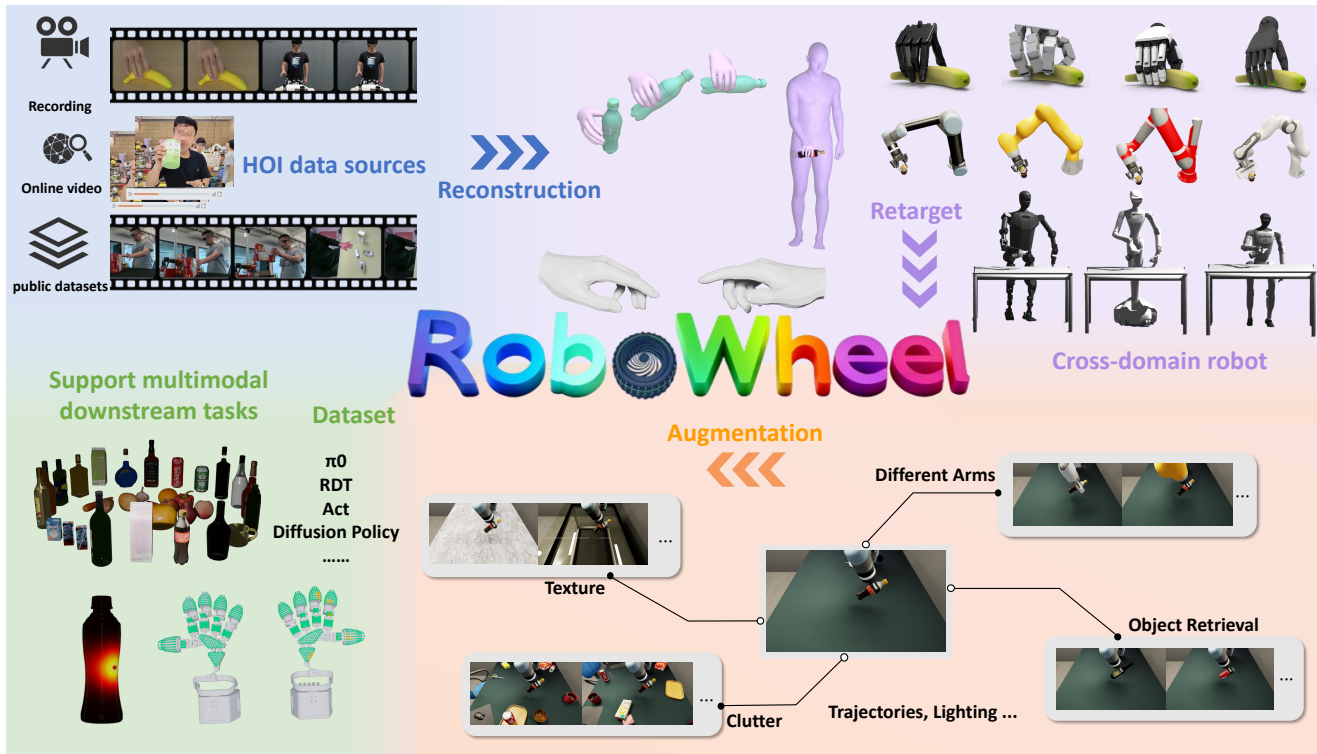


Figure 1. The *RoboWheel* data engine. Our pipeline could process hand-object interaction (HOI) videos from diverse sources (e.g., recordings and public datasets) through high-fidelity reconstruction to recover physically consistent trajectories. The reconstructed motions are retargeted to cross-domain robotic embodiments (e.g., arms, dexterous hands, humanoids), and enhanced with multi-modal data augmentations (e.g., object retrieval, texture, trajectories). This generates a large-scale dataset with multimodal observations, supporting training for various vision-language-action (VLA) and imitation learning models (e.g., ACT, Diffusion Policy).

## Abstract

We introduce **RoboWheel**, a data engine that converts human hand-object interaction (HOI) videos into training-ready supervision for cross-morphology robotic learning. From monocular RGB/RGB-D inputs, we perform high-

precision HOI reconstruction and enforce physical plausibility via a reinforcement learning (RL) optimizer that refines hand-object relative poses under contact and penetration constraints. The reconstructed, contact-rich trajectories are then retargeted to cross-embodiments, robot arms with simple end-effectors, dexterous hands, and humanoids, yielding executable actions and rollouts. To scale coverage, we build a simulation-augmented framework on Isaac Sim

\*Equal contribution, †Corresponding author. Work done by Yuhong Zhang, Zihan Gao during the internship at Synapath Research.

with diverse domain randomization (embodiments, trajectories, object retrieval, background textures, hand motion mirroring), which enriches the distributions of trajectories and observations while preserving spatial relationships and physical plausibility. The entire data pipeline forms an end-to-end pipeline from video  $\rightarrow$  reconstruction  $\rightarrow$  retargeting  $\rightarrow$  augmentation  $\rightarrow$  data acquisition. We validate the data on mainstream vision–language–action (VLA) and imitation learning architectures, demonstrating that trajectories produced by our pipeline are as stable as those from teleoperation and yield comparable continual performance gains. To our knowledge, this provides the first quantitative evidence that HOI modalities can serve as effective supervision for robotic learning. Compared with teleoperation, *RoboWheel* is lightweight: a single monocular RGB(D) camera is sufficient to extract a universal, embodiment-agnostic motion representation that could be flexibly retargeted across embodiments. We further assemble a large-scale multimodal dataset combining multi-camera captures, monocular videos, and public HOI corpora for training and evaluating embodied models.

## 1. Introduction

Embodied agents learn most effectively when their supervision matches how humans interact with the world. However, obtaining specific robot-usable supervision at scale is challenging. Existing data collection pipelines mainly rely on teleoperation or studio motion capture, which demands specialized hardware and careful curation, limiting the diversity of action behaviors and their transferability across robot embodiments and tasks. At the same time, multiple data sources provide vast amounts of hand–object interaction (HOI) information containing rich and real-world manipulation strategies, yet these signals are rarely converted into training-ready data for robots due to reconstruction noise, physical implausibility, and embodiment mismatch.

Recent advances in human- and object-centric perception suggest an opportunity to close this gap. Methods based on SMPL-H/MANO [46, 48, 50] and 6D object pose or mesh tracking [39, 40, 47] can recover detailed geometry and motion from monocular RGB/RGB-D inputs. Nevertheless, contact estimates are often inconsistent, hand–object interpenetrations arise under occlusion, trajectories lack temporal smoothness, and the recovered motions generally violate kinematic and dynamic constraints.

Bridging this gap requires a practical, scalable processing pipeline that satisfies three key requirements: (i) enabling large-scale, continuous acquisition of robot–object interaction trajectories in real-world operational spaces while enforcing physical plausibility; (ii) supporting flexible retargeting of these trajectories to diverse robot embodiments—even across domains—while preserving interaction semantics; and (iii) maintaining scalability by enabling ef-

fective composition of data augmentation strategies. Existing paradigms for robot data collection—teleoperation and simulated data generation—fail to meet these requirements jointly: teleoperation is costly and hardware-specific, whereas purely synthetic simulation data often does not reflect real-world perceptual and contact distributions.

We address these challenges with *RoboWheel*, a data engine that transforms real-world hand–object demonstrations into supervision for cross-embodiment robotic learning. Starting from monocular RGB(D) HOI videos, *RoboWheel* integrates state-of-the-art hand, body, and object motion estimators into a unified reconstruction framework. A multi-stage physical plausibility optimization then refines the trajectories: signed distance function (SDF)-based penalties discourage interpenetration and encourage contact, and a residual reinforcement learning (RL) policy further adjusts hand–object relative poses under reachability and stability priors. The resulting trajectories are mapped into a canonical action space and retargeted to heterogeneous robot morphologies—including 6/7-DoF arms with parallel grippers, dexterous hands, and humanoids, and output executable control sequences in both operational and joint spaces.

To scale coverage while preserving interaction semantics, we replay the retargeted trajectories in simulation across multiple robotic arms using GPU-accelerated parallel inverse kinematics. Within this environment, we apply domain randomization and diverse augmentations for observation and robotic action, including embodiment variations, trajectory distribution enrichment, object retrieval and replacement, background texture randomization, cluttered table configurations, hand mirroring, and more.

On top of this engine, we construct *HORA* (Hand–Object to Robot Action dataset), a large-scale multimodal dataset from three sources: a custom multi-view motion capture system with tactile-sensor gloves, an RGB(D) HOI recording setup, and multiple public HOI datasets. As a multimodal dataset, *HORA* combines the data modalities of HOI corpora and embodied robot datasets and *HORA* supports both HOI-related analysis and downstream robotic learning.

In summary, our key contributions as follows.

- **Physically plausible HOI reconstruction and cross-domain retargeting.** A monocular RGB/RGB-D HOI reconstruction framework that integrates state-of-the-art hand, body, and object motion estimation with physics-based optimization. The framework supports flexible cross-embodiment retargeting, outputs executable motion trajectories, and provides scalable supervision signals for downstream learning.
- **Simulation-augmented data flywheel.** We implement rich augmentation and domain randomization in simulation driven by HOI data. This data flywheel is validated on mainstream VLA and imitation learning models, and we conduct a quantitative evaluation of the quality and

effectiveness of both the HOI transformation and the augmentation strategy.

- **Large-scale multimodal dataset.** A multimodal dataset of over 150,000 sequences is constructed from multi-view motion capture, public HOI datasets, and recorded videos. It includes embodiment trajectories, observations, assets, HOI annotations, and task descriptions, with a mocap-based subset also providing tactile signals, offering a rich and scalable resource for robotic learning and downstream HOI-related tasks.

## 2. Related Work

**HOI datasets and monocular reconstruction.** High-precision HOI annotations remain costly, as most public 3D HOI datasets rely on multiview rigs or motion capture (MoCap) systems for accurate hand-object geometry [5, 14, 15, 33, 37]. Large egocentric video corpora like [13] use head-mounted cameras to avoid MoCap but lack frame-accurate 3D HOI geometry for reconstruction [12]. Recent whole-body motion datasets such as [49] scale to millions of SMPL-X frames but are not dedicated HOI datasets and offer limited hand-object contact supervision. On the algorithmic side, [8] reconstructs objects by fusing pixel-aligned features with 3D hand geometry in a transformer-based coarse-to-fine point cloud decoder, yielding dense object geometry with high frame fidelity, while [11] jointly reconstructs articulated hands and objects using compositional SDF and contact constraints. These methods, however, are generally limited to single-frame or in-contact scenarios and struggle with approach/withdrawal phases, generalizability, occlusion, low video resolution, and varying hand movement speeds. Recently, more generalizable approaches [30, 31, 43] have used data-driven priors; for instance, [43] introduces diffusion-guided, per-video optimization to enhance robustness under occlusion, albeit at the cost of heavier computation and the need for short clips.

**Robotic Learning from Human Demonstration** Early work in vision-based programming by demonstration mapped human hand poses to robot grasps directly from images, establishing a pipeline from grasp recognition to example-based robot execution [20]. More recent systems leverage richer HOI signals: [53] extract binocular hand-motion cues from human videos, compress trajectories into keyframes with coordination masks, augment demonstrations geometrically, and train a bimanual diffusion policy that executes long-horizon dual-arm tasks and generalizes across scenes. Complementarily, [38] treat human gestures as structured priors, retrieving grasp affordances from HOI memories and transferring them to novel objects, yielding robust performance in single-object and cluttered settings. At scale, cross-embodiment corpora and models (Open X-Embodiment/RT-X) demonstrate positive transfer across heterogeneous robots, motivating retargetable super-

vision from human interactions [36]. Specialized transfer frameworks extend this idea to dexterous bimanual manipulation via residual learning [23], while whole-body humanoid control benefits from motion-tracking pipelines distilled into guided diffusion policies that enable versatile downstream behaviors [35]. Together, these threads indicate a viable route from human HOI video to robot-useable policies via reconstruction, retargeting, and augmentation.

**Embodied models and scalable data for generalist manipulation.** Generalist *vision–language–action* policies pretrained on large video and robot corpora to enable instruction following and out-of-distribution generalization across tasks and embodiments [2, 3, 19, 54]. In parallel, imitation- and diffusion-based visuomotor learning emphasize stable training and multimodal action distributions, from classic action-diffusion policies to large diffusion foundation models that scale to bimanual control [9, 26]. To reduce data and hardware barriers, low-cost bimanual tele-operation systems provide dense demonstrations for fine-grained skills [51], while object-/pose-centric representations and semantic flows improve cross-object generalization and pose awareness [7]. At the dataset/benchmark layer, dual-arm generators and domain-randomized platforms supply scalable supervision with unified evaluation [6, 27]; open-instruction rearrangement benchmarks probe 6-DoF reasoning under language guidance [10]; and video-driven pipelines synthesize long-horizon tasks directly from Internet videos [44]. Recent work on task-centric *latent actions* further mitigates embodiment mismatch by learning instruction-conditioned action spaces transferable across robots [4].

## 3. Method

### 3.1. System Overview

We build a systematic pipeline covering in-the-wild hand-object interaction(HOI) videos into robot-useable supervision data. Our pipeline overview is illustrated in Fig. 2.

### 3.2. HOI Reconstruction from RGB(D) videos

**Problem setup.** Given video frames  $\{I_t\}_{t=1}^T$ , our goal is to recover metrically consistent trajectories together with parametric representation of the hand and mesh of the manipulated object in the same world coordinate ,while (i) preventing hand–object interpenetration and (ii) enforcing physically plausible, temporally stable contact.Concretely, the state of the hand pose at time  $t$  is,

$$\mathbf{h}_t = (\theta_h(t), \mathbf{R}_h^w(t), \mathbf{t}_h^w(t)), \quad (1)$$

where  $\theta_h(t)$  is the hand pose,  $\mathbf{R}_h^w(t)$  and  $\mathbf{t}_h^w(t)$  are the global transform and wrist of hands in the world coordinate. The object state is the rigid 6D pose tied to its (scale-resolved) geometry,  $\mathbf{p}_t = T_o^w(t) \in \text{SE}(3)$ , defines the location and rotation of the object.

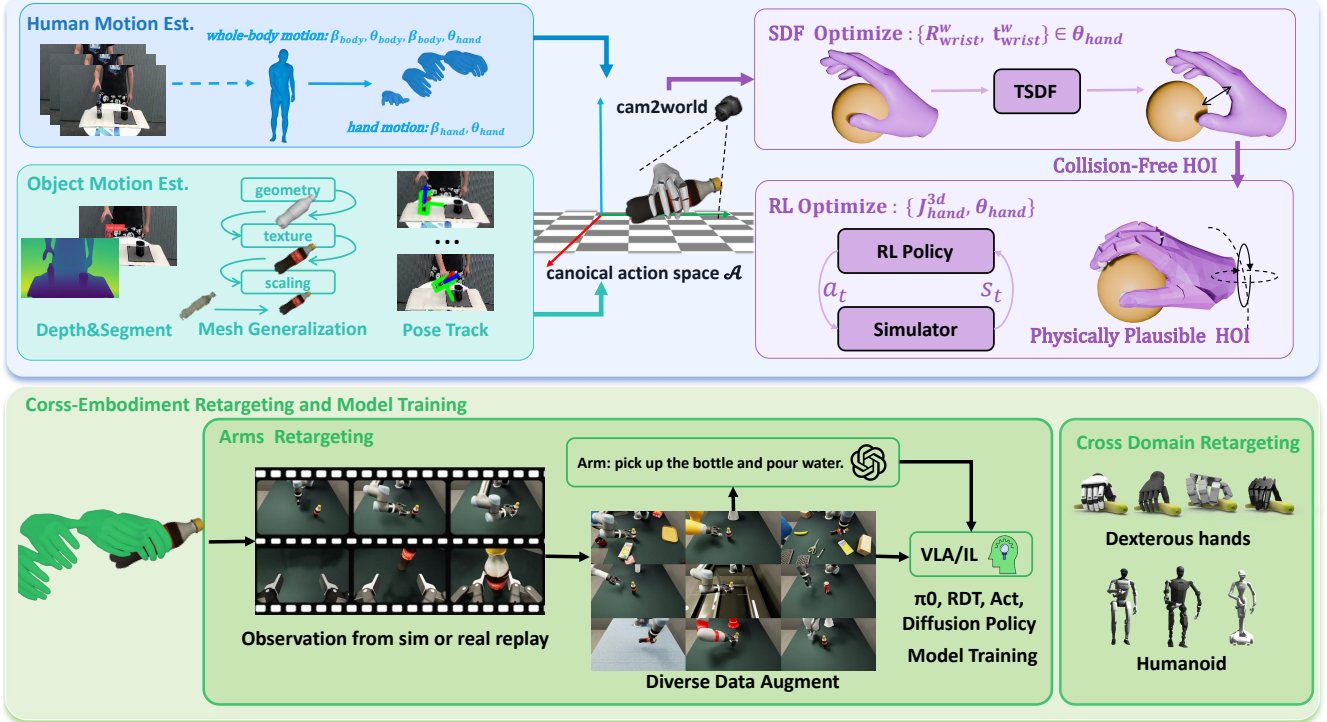


Figure 2. Given monocular RGB(-D) input, we first estimate the motion of the hand or wholebody and the manipulated object. We then perform a joint optimization, guided by TSDF and reinforcement learning, to improve physical plausibility and ensure robotic reachability. The resulting trajectories are retargeted to heterogeneous embodiments—including arms, dexterous hands, and humanoids. Finally, domain randomization for both observation and trajectories in Isaac Sim is applied to enrich observational diversity for robotic arms, and the generated embodied data is validated across both VLA and IL policy benchmarks.

**Human and hand motion recovery.** Our method initially determines whether a clip implies *hand-only* or *whole-body* motion. For the *hand-only* case, we estimate  $\mathbf{h}_t$  per frame using [28]. Otherwise, we estimate the SMPL-H parameters via [49] and directly produce the world coordinate body pose  $\theta_b(t)$  and the shape  $\beta_b$ , equivalently extracting the hand state  $\mathbf{h}_t$ .

**Object reconstruction and pose estimation.** We ground the manipulated object, obtaining the per-frame mask  $m_t$  and depth  $D_t$  (predicted by [29] or RGB-D) in the video. Conditioned on semantic cues, we use a multiview 3D generator  $\mathcal{G}$  [52] to produce an unscaled textured mesh  $\hat{M}_o$ . Then we recover the metric scale of the manipulated object by back-projecting the depth map inside the mask to a point set  $\mathcal{P}_t = \{X_c(p) = D_t(p) K^{-1} \tilde{p} \mid p \in m_t\}$ , aggregating as  $\mathcal{P} = \bigcup_t \mathcal{P}_t$ . We obtain the rescaled object mesh  $M_o$  via  $M_o = s_o \hat{M}_o$ , where  $s_o$  denotes the ratio between the diagonals of the bounding boxes of  $\mathcal{P}$  and  $\hat{M}_o$ . With  $(M_o, M_t, D_t)$ , a correspondence-driven tracker  $\mathcal{F}(\cdot)$  [39] estimates the pose stream of the camera frame object  $T_o^c(t)$ .

To eliminate viewpoint-dependent inconsistencies in real-world HOI videos, we first estimate the camera intrinsics  $K$  and the camera-to-world transformation  $T_c^w = (R_{wc}, t_{wc})$  using [34]. This allows us to transform all reconstructed hand-object interactions to the world coordinate

system. We then align the resulting trajectories to a **canonical action space**  $\mathcal{A}$  by constructing a reference frame based on body joint positions, ensuring consistency across heterogeneous sources. For detailed transformation steps, please refer to Appendix.

**Optimization for physical plausibility.** Let  $\phi_o(\mathbf{x}; t)$  be a watertight object Truncated Signed Distance Function (TSDF, positive outside), and hand vertices  $V_h$ . First, we optimize the hand parameter  $\mathbf{t}_h^w$  to avoid penetration between object and hand-palm by minimizing  $\phi_o^2(V_h^{palm}, t)$ .

As shown in the upper-right corner of Fig. 2, we then optimize the hand parameters  $\mathbf{R}_w^w, \mathbf{t}_w^w \in \theta_h$ , to avoid hand-object interpenetration. Detailed collision optimization strategy is described in the supplementary material.

With collision-free HOI initialization, we introduce a residual RL policy [22] to obtain physically plausible hand-object poses while ensuring reachability on the robot. Specifically, a residual learning strategy is applied to refine the trajectories of both the hand and the object. The RL policy then encourages accurate tracking of these refined trajectories while promoting physically consistent contact once the hand-object distance drops below a threshold. The resulting state after RL is denoted as  $s_t = (h_t, p_t, \dot{h}_t, \dot{p}_t, \mathcal{C}_t)$ . Here,  $h_t, p_t$  denote the hand poses and object poses, respectively, along with their corresponding

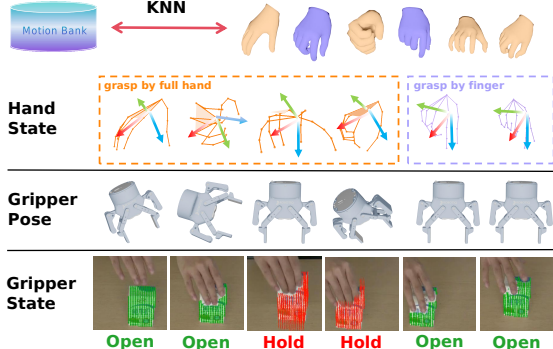


Figure 3. Map the hand’s joints to the gripper’s end-effector pose, including the corresponding mapping of the gripper’s opening and closing state.

velocities and  $\mathcal{C}_t$  denotes the contact force. Reward function  $r_t$  is defined as follows:

$$r_t = \lambda_{\text{geo}} \Phi_{\text{geo}} (\|\Delta h_t\| + \|\Delta p_t\|) + \lambda_{\text{dyn}} \Phi_{\text{dyn}} (\|\Delta \dot{h}_t\| + \|\Delta \dot{p}_t\|) + \lambda_{\text{con}} \Phi_{\text{con}} (\mathcal{C}_t), \quad (2)$$

where  $\Phi$  denotes the reward function and  $\Delta$  denotes the error between resulting states  $s_t$  and target states.

### 3.3. Cross-Embodiment Retargeting

Based on the physically plausible joint HOI reconstruction in Section 3.2, we obtained physically plausible trajectories  $\{h_t, p_t\}_{t=1}^T$  and ensured stable hand-object contacts. We aim to retarget these to heterogeneous robot embodiments—industrial arms, dexterous hands, and humanoids.

**Robot arms.** Given accurate 3D hand joints, we retarget hand poses into executable end-effector poses  $\{T_g(t), g(t)\}_{t=1}^T$  for a parallel-jaw gripper (Fig. 3). Inspired by [21], we implement two complementary orientation constructions depending on whether the *whole hand* (palm-involved) or *only finger tips* dominate the contact geometry. We use a kNN classifier to determine the gesture category. *Whole-hand* retargeting builds a stable palm frame from MCP joints to suppress fingertip jitter; *finger-only* mapping aligns to a hand-intrinsic frame and uses the index–thumb chord to define the gripper axis. For the detailed retargeting algorithm, please refer to the Appendix. To assess the state of the gripper, we employ CoTracker [17] to track the motion trajectories of key points on the manipulated object. The gripper state is determined based on the displacement of these key points. If these points remain stationary, the gripper is classified as open; otherwise, it is classified as closed. By focusing on keypoints rather than the object’s mask, this approach achieves robustness to the visual ambiguity induced by severe occlusions during manipulation. We subsequently conducted real-robot experiments on a UR5 robotic arm equipped with a parallel gripper to validate the effectiveness of this retargeting method.

**Dexterous hands and humanoids.** Beyond retargeting to simple gripper-based arms, our high-fidelity HOI recon-

struction offers a glimpse into transferring human demonstrations to more complex embodiments, including dexterous hands and humanoid robots. For dexterous hands, we retarget the reconstructed hand motions to the joint space of target robotic hands using kinematic similarity and contact-preserving constraints. For whole-body human demonstrations, we extend retargeting to humanoid platforms by leveraging full-body SMPL-H estimates. The resulting motion sequences are adapted to humanoid joint trees through inverse kinematics and dynamics-aware optimization, ensuring physical plausibility and intent preservation. Preliminary validations are provided in the Appendix.

**Replay Assessment and Language Caption** When replaying trajectories in simulation, executions may fail due to precision or non-physical collisions in the physics engine. To mitigate this, we employ Qwen2.5 VL [1] for automatic binary task evaluation (success/failure). The model takes as input the task description along with both wrist- and third-view simulated observations to determine whether the action has been successfully completed. For trajectories deemed successful, we further derive and refine fine-grained language instructions using [16].

### 3.4. Data Augmentation in Simulation

While preserving contact semantics and physical plausibility that are critical for embodiment control, we perform extensive simulation-based data augmentation to enrich the diversity of visual observations and motion trajectories. All augmentation strategies are applied within the canonical action space  $\mathcal{A}$  to handle different manipulation orientations. More visualizations are provided in the Appendix.

**Different types of arm retargeting.** Given an executable end-effector (EE) trajectory  $\{T_g(t)\}$  produced by our retargeting method, we generate observations for heterogeneous arms, as illustrated in Fig. 4. In Isaac Sim, we instantiate five widely used 6/7-DoF robotic arms as simulation assets, including *UR5/UR5e*, *Franka Emika Panda*, *KUKA LBR iiwa 7*, *Kinova Gen3*, and *Rethink Robotics Sawyer*. HOI-derived 6D EE trajectories  $T_g(t) \in \text{SE}(3)$ ,  $t = 1, \dots, T$ , are mapped into feasible joint trajectories using cuRobo’s GPU-accelerated inverse kinematic (IK) backend [32]. For each robotic arm, at every timestep we invoke IK solver with the target pose  $T_g(t)$ . The solver returns a feasible joint configuration:

$$q_t = \arg \min_q \mathcal{C}_{\text{goal}}(T_g(t), q) \quad (3)$$

$$\text{s.t. } q_{\min} \preceq q \preceq q_{\max}, \mathcal{C}_{\text{coll}}(q) \leq 0,$$

where  $\mathcal{C}_{\text{goal}}$  is cuRobo’s pose reaching cost and  $\mathcal{C}_{\text{coll}}$  is the self-collision constraint. To encourage temporal consistency, we use the previous solution  $q_{t-1}$  as the IK seed when invoking the solver.

Episodes that pass the replay check preserve the original HOI intent (e.g., grasp/place/pour) while providing embod-

iment diversity in joint space. We export both the joint-space commands  $\{q_t\}_{t=1}^T$  (arm and gripper included) and aligned operational-space labels per robot, enabling multi-morphology policy training from the same HOI source.

**Object retrieval and replacement.** We build a large object library by combining [52] generations with in-house scans; each asset includes a watertight mesh, texture, category tag, and a canonical pose. For a source episode with object mesh  $M_o$  and object pose stream  $\{T_o(t)\}$ , we retrieve top- $K$  substitutes  $\tilde{M} = \{\tilde{M}_k\}$  using a fused similarity,

$$\begin{aligned} \mathcal{S}(M_o, \tilde{M}) = & \alpha \text{CD}(\hat{M}_o, \hat{\tilde{M}}) + \beta (1 - \text{IoU}_{\text{AABB}}) \\ & + \gamma \langle \phi_{\text{sem}}(M_o), \phi_{\text{sem}}(\tilde{M}) \rangle, \end{aligned} \quad (4)$$

where  $\hat{\cdot}$  denotes unit AABB normalization, CD is the symmetric Chamfer distance on surface samples,  $\text{IoU}_{\text{AABB}}$  measures coarse shape compatibility, and  $\phi_{\text{sem}}$  are text-shape embeddings.

To ensure replay compatibility on a retrieved substitute, we align principal axes and bind the same maximum AABB and canonical pose definition as the source  $M_o$ . Under this binding, the original EE motion plan and the hand-object interaction geometry remain consistent, so the control trajectory can be directly replayed on geometrically/semantically matched novel objects (e.g., mug  $\leftrightarrow$  cup-with-handle, box  $\leftrightarrow$  carton).

**Trajectory augmentation.** Informed by [41] and tailored to our setting, we represent each demonstration as a trajectory  $\tau = \{(T_g(t), g(t))\}_{t=1}^T$ , where  $T_g(t) = (R(t), p(t)) \in \text{SE}(3)$  denotes the EE pose with orientation  $R(t)$  and translation  $p(t)$ , and  $g(t)$  is the gripper command. The trajectory is partitioned into object-centric segments  $\{\tau^{(k)}\}$ , each labeled by a contact state  $c^{(k)} \in \{\text{hold}, \text{open}\}$ . Instead of re-planning trajectories, we augment them as follows.

(i) For interaction segments ( $c^{(k)} = \text{hold}$ ), we apply an object-frame rigid transform  $T_o \in \text{SE}(3)$  to each waypoint:

$$\tilde{T}_g(t) = T_o T_g(t), \quad \tilde{g}(t) = g(t).$$

Let  $R_\Delta := \text{Rot}(T_o)$ . To maintain continuity without motion-plan regeneration, the same EE orientation change is applied to non-interaction segments (see (ii)), and the orientation change induced by  $R_\Delta$  is kept small for IK feasibility and repeatable execution.

(ii) For each non-interaction segment ( $c^{(k)} = \text{open}$ ), we linearly remap the translational path and set the EE orientation as  $\tilde{R}(t) = R_\Delta R(t)$ . Let  $p_s, p_e$  be the original endpoints and  $\hat{p}_s, \hat{p}_e$  the remapped anchors: the anchor adjacent to a transformed interaction segment is fixed by that segment, while the opposite anchor is chosen within a pre-defined reachable set. With  $\alpha_t \in [0, 1]$  denoting the normalized progress along the original segment from  $p_s$  to  $p_e$ ,

$$\tilde{p}_t = \hat{p}_s + \alpha_t(\hat{p}_e - \hat{p}_s) + \left[ p_t - (p_s + \alpha_t(p_e - p_s)) \right]. \quad (5)$$

## 4. Dataset

Using the *RoboWheel* pipeline, we build a large-scale multimodal HOI-robotic dataset ***HORA***. The dataset integrates multiple data sources and leverages successive stages of the *RoboWheel* to convert heterogeneous inputs into a unified hoi representation, followed by cross-embodiment retargeting and diversified data augmentation. Data sources include: (i) a custom multi-view mocap system equipped with tactile sensor-instrumented gloves, (ii) multiple public HOI datasets, and (iii) a custom RGB(D) video capture setup. For source (i), high-precision HOI signals are obtained via triangulation and FoundationStereo [40], while the remaining robot-relevant modalities are generated using the *RoboWheel* retargeting and augmentation pipeline. For source (ii), existing HOI modalities in public datasets are directly convert to the canonical action space  $\mathcal{A}$ , then retargeted and augmented in the same manner. For source (iii), the full *RoboWheel* pipeline processes raw videos to extract both HOI and embodied modalities. For detailed information on the tasks included in each subset, please refer to our Appendix. The following sections detail the modality composition and statistics of ***HORA***, as well as the acquisition system for the **mocap subset**.

### 4.1. Modalities Composition and Statistics.

As summarized in Tab. 1, *RoboWheel* produces a unified multimodal representation across the three subsets of ***HORA***. These modalities can be broadly grouped into two categories: those for HOI downstream tasks and those for robot-related tasks. The HOI modalities include sequences of hand MANO parameters (pose/shape with global orientation and translation) in world frame from the original data source, object 6dof pose, object assets, and hand-object contact annotations. The robot-related modalities include observations from the robot wrist and third-person viewpoints, as well as end-effector pose trajectories for the robotic arm. All trajectories are transformed into the canonical action space  $\mathcal{A}$ .

The **mocap subset** provides tactile signals, robotic observations, and HOI annotations. Concretely, we release the 6-DoF object pose, object assets, and a dense tactile map for both the hand and the object. The **recording subset** provides the same HOI and robotic modalities, except for tactile signals, because the collection setup did not include the hardware. The **public HOI subset** is constructed from existing HOI datasets [5, 15, 24, 33, 37] and currently includes the cross-embodiments modalities retargeted to different arms (6/7-DoF). The three subsets together constitute roughly 150k trajectories, distributed shown in Fig. 5.

### 4.2. Custom-built Mocap system

**Acquisition System** Our high-precision mocap subset is collected with a synchronized, multi-sensor capture rig, the data acquisition setup and tactile glove are shown in Fig. 6.

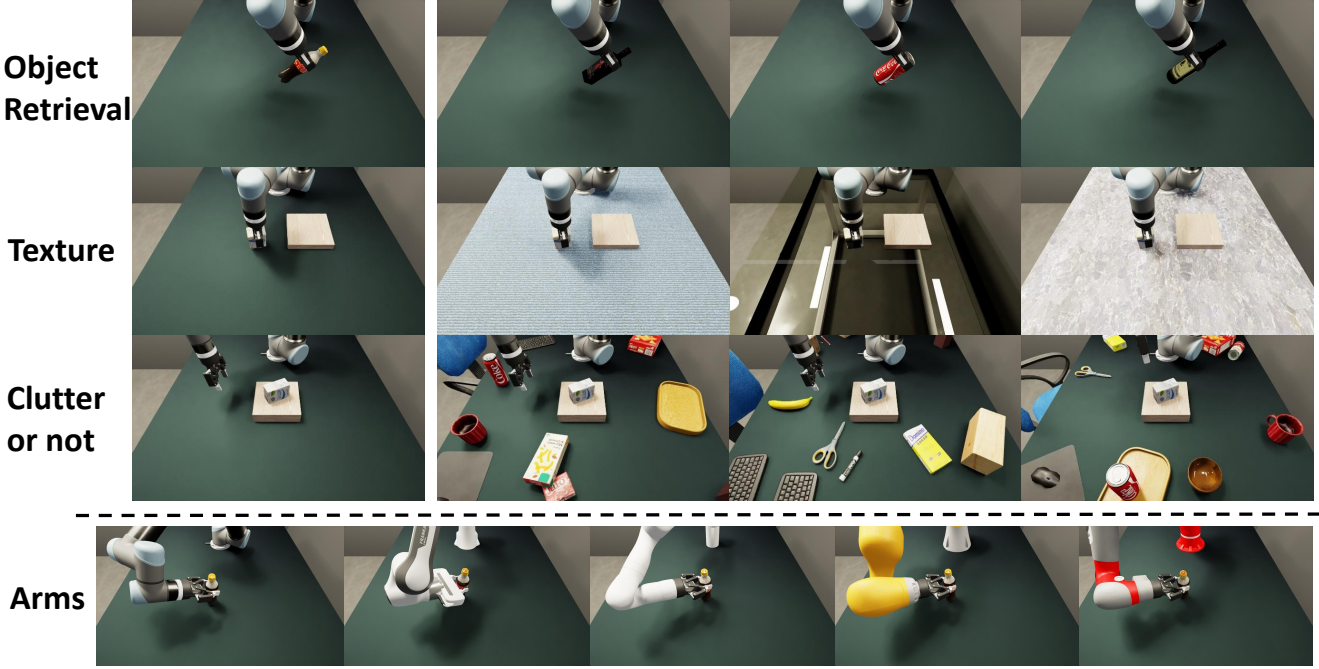


Figure 4. *RoboWheel* diverse augmentation in simulation.

Dataset	Tactile	Robotic data	HOI data	# Trajectories	Object Info Granularity
GRAB [33]	✗	✗	✓	1334	6-DoF pose & Contact maps
HO3D (v3) [15]	✗	✗	✓	68	6-DoF pose & Assets
DexYCB [5]	✗	✗	✓	1,000	6-DoF pose & Assets
HO-Cap [37]	✗	✗	✓	~64	6-DoF pose & Assets
TACO [24]	✗	✗	✓	2,500	Assets
DROID [18]	✗	✓	✓	76,000	Assets
LIBERO [25]	✗	✓	✗	366	Assets
UCSD Kitchen [42]	✗	✓	✗	150	■
<b><i>HORA</i>(Recordings)</b>	✗	✓	✓	23560	6-DoF object pose & Assets
<b><i>HORA</i>(Mocap)</b>	✓	✓	✓	63141	6-DoF object pose & Assets & Tactile map
<b><i>HORA</i>(Public Dataset)</b>	✗	✓	✓	66924	■

Table 1. Modalities and scale comparison. For *HORA*, the first three rows correspond to our mocap, recorded RGB(D), and public HOI subsets. “✗” and “✓” denote absence and presence, respectively.



Figure 6. Data collection setup and tactile information.

We use three Intel RealSense D455 RGB-D cameras connected via hardware sync cables to obtain time-aligned, metric depth from multiple viewpoints, and eight additional RGB cameras, yielding up to eleven views for each interaction. All cameras are extrinsically calibrated into a common world coordinate frame and temporally synchronized with the hand instrumentation.

Hand motion and tactile sensing are recorded using **EVT2** developed by **Paxini**. The glove integrates

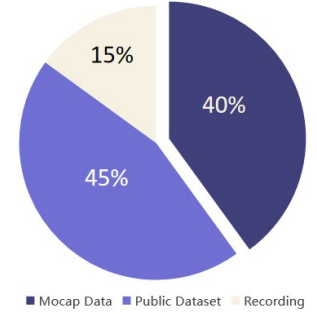


Figure 5. Composition of the three subsets in *HORA*.

- **29 magnetic encoders** distributed over the hand kinematic chain (wrist, palm, and phalanges), which provide joint-level pose measurements.
- **16 Gen3 tactile (haptic) sensors** mounted on key contact regions (fingertips, finger pads, and palm), which measure local normal forces.

These signals are used both for fitting MANO parameters and for deriving tactile and contact annotations that we release as part of the dataset.

**Fitting to MANO with tactile signals** We develop a tactile-guided, multi-constraint optimization scheme for motion retargeting. By registering glove measurements to the MANO hand model (or a target robot URDF) and jointly enforcing constraints on tactile contact states, wrist pose calibration, joint smoothness, and anatomical priors,

the system optimizes all frames in parallel to produce spatiotemporally consistent, tactile-synchronized, and physically plausible motion trajectories. See Appendix for implementation details of the retargeting algorithm.

## 5. Experiment

### 5.1. HOI Reconstruction Quality

We evaluate HOI reconstruction quality on [37] with common metrics in Sec. 5.1 and Fig. 7. All methods receive the same camera parameters and object meshes for a fair comparison. We compare *RoboWheel* with HORT [2025], HOLD [2023], and DiffHOI [2023].

### 5.2. Validation of *HORA* Data

Here we show how *HORA* data support downstream tasks and how well learned skills transfer with data augmentation.

**Performance on different VLA/IL models.** To study how Robowheel reconstructions translate to downstream control, we benchmark eight household tasks grouped by difficulty (Easy/Hard) and evaluate several VLA/IL algorithms (ACT, DP, RDT, Pi0). We evaluate each algorithm under three training regimes: (i) fine-tuning on 10 teleoperation demonstrations (tele.), (ii) fine-tuning on 10 *HORA* trajectories (*HORA*), and (iii) a two-stage curriculum that first pre-trains on 5k *HORA* trajectories and then fine-tunes on 10 *HORA* trajectories (reported as RDT+5k*HORA* and Pi0+5k*HORA*). The third training regime is applied only to RDT and Pi0, as the other methods do not support pre-training. Per-task success rate(%) is reported in the same real setup in Tab. 3. Macro averages within each difficulty group are reported. See Appendix for more results.

As shown in Tab. 3 and Fig. 8, VLA policies (Pi0 & RDT) pretrained with 5k *HORA* data achieved the highest success rates, demonstrating a remarkable performance improvement over counterparts without pretraining. The impact of this improvement is more evident in tasks of higher complexity. Notably, when training or fine-tuning these VLA/IL methods with an identical number of training episodes from teleoperation or *HORA*, policies trained solely on *HORA* achieve performance comparable to those trained on teleoperation data, despite the sim-to-real gap. The underlying reason for this is twofold. First, *RoboWheel* provides precise HOI reconstruction, enabling the generation of trajectories with accuracy approaching that of teleoperation, ensuring effective transfer from simulation to real-world environments. Second, data augmentation is applied to *HORA*, and its broader data distribution helps the policy mitigate the negative impact of the visual domain gap, endowing the policies with enhanced robustness.

**Impact of *HORA* on Model Robustness** To assess whether the data augmentation strategies in *HORA* enhance the robustness of VLAs, we compare RDT fine-tuned on *HORA* only (*HORA*) versus *HORA* with augmentation

(*HORA*-aug). Specifically, we select four tasks and conduct real-robot experiments under three distribution shifts: *unseen objects*, *unseen backgrounds*, and *cluttered scenes*. Each cell shows *successes/trials* for two independent runs, as shown in Tab. 4. When trained on the *HORA* without augmentation, the fine-tuned RDT still manages to achieve some successful trials when encountering unseen objects or inferring in cluttered environments. However, when the background is altered, inducing substantial changes in the observations, the model exhibits catastrophic degradation in performance. In contrast, the fine-tuned RDT with augmented *HORA* shows a significant improvement in handling new observations, particularly in the unseen background setting, where the success rate increased by 25%. These results demonstrate that training on *HORA*, particularly with augmentation, substantially enhances the robustness of VLA models to visual variations.

### 5.3. Real-robot replay performance comparison

Under the same hand joints sequence input, we retarget the motions to a two-finger gripper using both existing methods and our proposed approach as discussed in Sec. 3.3, executing an identical set of tasks and measuring success rates to quantitatively evaluate the robustness of each mapping scheme. As shown in Tab. 5, our retargeting method consistently achieves higher success rates across all manipulation tasks. Its refined formulation of gripper orientation proves more robust, enabling stable yet flexible execution under diverse and dynamic hand-gesture regimes.

## 6. Conclusion and Discussion

**Conclusion.** Our data engine, *RoboWheel*, transforms real-world HOI videos into cross-embodiment robotic learning supervision by integrating high-fidelity hand–object reconstruction, physically plausible trajectory optimization, and cross-embodiment retargeting. Leveraging unified HOI representation that is inherently robust to existing embodiment variations, *RoboWheel* provides a scalable framework for generating robotic training data. The framework is further strengthened with a rich suite of simulation-based data augmentation strategies. Based on two self-developed hardware platforms and existing public HOI datasets, we have constructed a large-scale HOI-to-Robot dataset *HORA*, which supports VLA models and imitation-learning approaches. Furthermore, our study establishes the first quantitatively validated evidence that HOI data can serve as an effective upstream modality for training models across diverse downstream, embodiment-specific tasks.

**Limitations and Future Work.** The scope of our real-world cross-embodiment experiments—particularly those involving dexterous hands and humanoid remains limited. Expanding cross-domain validation in both real-world and simulated settings will be an important direction in future.

Method	Object			Hand		Rel. pose consistency ↓	
	CD (cm)↓	F5 (%)↑	F10 (%)↑	Hand jitter (cm/s <sup>2</sup> )↓	W-MPJPE (mm)↓	Trans (cm)↓	Rot (deg)↓
HORT	8.9	55.0	83.0	3.35	19.92	3.54	-
DiffHOI	7.2	59.6	78.1	4.59	20.21	4.51	-
HOLD	7.5	53.2	77.9	3.47	20.59	2.44	-
<b>Ours</b>	<b>5.1</b>	<b>63.4</b>	<b>89.1</b>	<b>0.92</b>	<b>7.81</b>	<b>0.26</b>	<b>1.9</b>

Table 2. HOI reconstruction quality comparison. **Object surface:** CD (cm) = bidirectional Chamfer distance; F5/F10 (%) = F-score at 5/10 mm. **Hand:** Hand jitter (cm/s<sup>2</sup>) = time-avg. norm of frame-to-frame wrist/palm acceleration (30 FPS, 2nd-order diff.); W-MPJPE (mm) = world frame MPJPE. **Rel. pose consistency:** std of  $T_{\text{rel}}(t) = T_h^{-1}(t)T_o(t)$  in translation (cm) / rotation (deg).

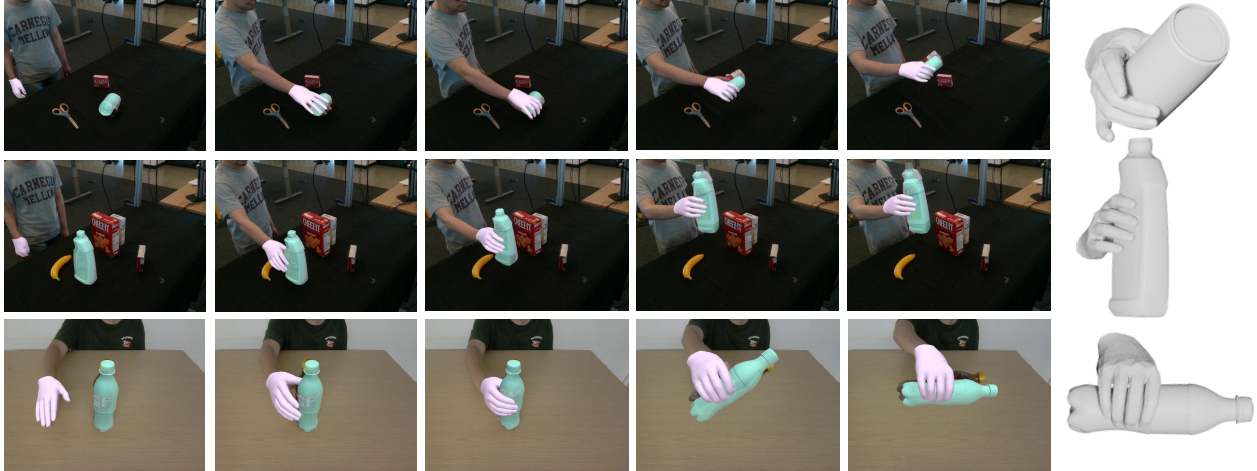


Figure 7. HOI reconstruction results of *RoboWheel*. Whether the data comes from public HOI datasets (e.g., DexYCB) or not, *RoboWheel* can achieve high-precision HOI reconstruction.

Real-world Tasks	Diff.	ACT		DP		RDT		Pi0		RDT+5kHORA		Pi0+5kHORA	
		tele.	HORA	tele.	HORA	tele.	HORA	tele.	HORA	HORA	HORA	HORA	HORA
Pick up milk	Easy	15.0	0.0	20.0	15.0	55.0	30.0	70.0	65.0	<b>70.0</b>	<b>80.0</b>		
Lift wooden cup		0.0	0.0	45.0	25.0	75.0	45.0	65.0	55.0	<b>70.0</b>	<b>70.0</b>		
Place milk		35.0	0.0	50.0	35.0	70.0	50.0	80.0	55.0	<b>85.0</b>	<b>80.0</b>		
Restore bowl		0.0	0.0	5.0	0.0	65.0	65.0	60.0	60.0	<b>75.0</b>	<b>75.0</b>		
Average		12.5	0.0	30.0	18.8	66.3	47.5	68.8	58.8	<b>75.0</b>	<b>76.3</b>		
Move banana	Hard	0.0	0.0	5.0	0.0	55.0	20.0	40.0	15.0	<b>65.0</b>	<b>60.0</b>		
Upright milk		0.0	0.0	0.0	15.0	45.0	30.0	60.0	50.0	<b>60.0</b>	<b>75.0</b>		
Pour cola		0.0	0.0	0.0	10.0	35.0	35.0	25.0	35.0	<b>40.0</b>	<b>55.0</b>		
Tip teacup		0.0	0.0	0.0	0.0	5.0	15.0	35.0	25.0	<b>25.0</b>	<b>45.0</b>		
Average		0.0	0.0	1.3	6.3	35.0	25.0	40.0	31.3	<b>47.5</b>	<b>58.8</b>		

Table 3. Real-world task performance (%) grouped by difficulty.

## Acknowledgement

zhen Science and Technology Project under Grant (KJZD20240903103210014).

This research was funded through the National Key Research and Development Program of China (Project No. 2022YFB36066), in part by the Shen-

Real-world Tasks	Unseen Object		Clutter Objects		Unseen Background	
	HORA	HORA-aug	HORA	HORA-aug	HORA	HORA-aug
Lift wooden cup	4/10	<b>5/10</b>	4/10	<b>4/10</b>	0/10	<b>4/10</b>
Place milk	5/10	<b>6/10</b>	5/10	<b>6/10</b>	1/10	<b>3/10</b>
Upright milk	3/10	<b>3/10</b>	4/10	<b>4/10</b>	3/10	<b>5/10</b>
Pour cola	3/10	<b>3/10</b>	3/10	<b>4/10</b>	2/10	<b>4/10</b>
Average	3.75/10	<b>4.25/10(+0.5)</b>	4.00/10	<b>4.50/10(+0.5)</b>	1.50/10	<b>4.00/10(+2.5)</b>

Table 4. Task performance in unseen scenarios with RDT.



Figure 8. Real-world Performance on 4 Tasks.

## References

- [1] Shuai Bai, Keqin Chen, Xuejing Liu, Jialin Wang, Wenbin Ge, Sibo Song, Kai Dang, Peng Wang, Shijie Wang, Jun Tang, et al. Qwen2. 5-vl technical report. *arXiv preprint arXiv:2502.13923*, 2025. [5](#)
- [2] Kevin Black, Noah Brown, James Darpinian, Karan Dhabalia, Danny Driess, Adnan Esmail, Michael Equi, Chelsea Finn, Niccolò Fusai, Manuel Y Galliker, et al.  $\pi$ 0. 5: a vision-language-action model with open-world generalization. *arXiv preprint arXiv:2504.16054*, 2025. [3](#)
- [3] Anthony Brohan, Noah Brown, Justice Carbajal, Yevgen Chebotar, Joseph Dabis, Chelsea Finn, Keerthana Gopalakrishnan, Karol Hausman, Alex Herzog, Jasmine Hsu, et al. Rt-1: Robotics transformer for real-world control at scale. *arXiv preprint arXiv:2212.06817*, 2022. [3](#)
- [4] Qingwen Bu, Yanting Yang, Jisong Cai, Shenyuan Gao, Guanghui Ren, Maoqing Yao, Ping Luo, and Hongyang Li. Univla: Learning to act anywhere with task-centric latent actions. *arXiv preprint arXiv:2505.06111*, 2025. [3](#)
- [5] Yu-Wei Chao, Wei Yang, Yu Xiang, Pavlo Molchanov, Ankur Handa, Jonathan Tremblay, Yashraj S. Narang, Karl Van Wyk, Umar Iqbal, Stan Birchfield, Jan Kautz, and Dieter Fox. Dexycb: A benchmark for capturing hand grasping of objects. In *Proceedings of the IEEE/CVF Conference on Computer Vision and Pattern Recognition (CVPR)*, pages 9044–9053, 2021. [3, 6, 7](#)
- [6] Tianxing Chen, Zanxin Chen, Baijun Chen, Zijian Cai, Yibin Liu, Qiwei Liang, Zixuan Li, Xianliang Lin, Yiheng Ge, Zhenyu Gu, et al. Robotwin 2.0: A scalable data generator and benchmark with strong domain randomization for robust bimanual robotic manipulation. *arXiv preprint arXiv:2506.18088*, 2025. [3](#)
- [7] Tianxing Chen, Yao Mu, Zhixuan Liang, Zanxin Chen, Shijia Peng, Qiangyu Chen, Mingkun Xu, Ruizhen Hu, Hongyuan Zhang, Xuelong Li, et al. G3flow: Generative 3d semantic flow for pose-aware and generalizable object manipulation. In *Proceedings of the Computer Vision and Pattern Recognition Conference*, pages 1735–1744, 2025. [3](#)
- [8] Zerui Chen, Rolandoz Alexandros Potamias, Shizhe Chen, and Cordelia Schmid. Hort: Monocular hand-held objects reconstruction with transformers. *arXiv preprint arXiv:2503.21313*, 2025. [3, 8](#)
- [9] Cheng Chi, Zhenjia Xu, Siyuan Feng, Eric Cousineau, Yilun Du, Benjamin Burchfiel, Russ Tedrake, and Shuran Song. Diffusion policy: Visuomotor policy learning via action diffusion. *The International Journal of Robotics Research*, page 02783649241273668, 2023. [3](#)
- [10] Yufei Ding, Haoran Geng, Chaoyi Xu, Xiaomeng Fang, Jiazhao Zhang, Songlin Wei, Qiyu Dai, Zhizheng Zhang, and He Wang. Open6dor: Benchmarking open-instruction 6-dof object rearrangement and a vlm-based approach. In *2024 IEEE/RSJ International Conference on Intelligent Robots and Systems (IROS)*, pages 7359–7366. IEEE, 2024. [3](#)
- [11] Zicong Fan, Maria Parelli, Maria Eleni Kadoglou, Xu Chen, Muhammed Kocabas, Michael J Black, and Otmar Hilliges. Hold: Category-agnostic 3d reconstruction of interacting hands and objects from video. In *Proceedings of the IEEE/CVF Conference on Computer Vision and Pattern Recognition*, pages 494–504, 2024. [3](#)
- [12] Kristen Grauman, Michael Wray, Adriano Fragomeni, Jonathan P. N. Munro, Will Price, Pablo Arbelaez, David Crandall, Dima Damen, Giovanni Maria Farinella, Bernard

Task	Ours	GAT-Grasp	yoto
Lift wooden cup	<b>87.5</b>	25.0	75.0
Place bowl	<b>100</b>	62.5	100
Upright milk	<b>100</b>	50.0	62.5
Pour cola	<b>100</b>	62.5	75.0
move banana	<b>87.5</b>	62.5	87.5
Tip teacup	<b>87.5</b>	37.5	00.0
Macro avg	<b>91.7</b>	50.0	66.7

Table 5. Robot **direct replay** success rate  $\uparrow$  (%).

Ghanem, C. V. Jawahar, Kris M. Kitani, Aude Oliva, Hyun Soo Park, James M. Rehg, Yoichi Sato, Mike Zheng Shou, Antonio Torralba, Jitendra Malik, et al. Ego4d: Around the world in 3,000 hours of egocentric video. In *Proceedings of the IEEE/CVF Conference on Computer Vision and Pattern Recognition (CVPR)*, pages 18973–18990, 2022. 3

[13] Kristen Grauman, Andrew Westbury, Lorenzo Torresani, Kris Kitani, Jitendra Malik, Triantafyllos Afouras, Kumar Ashutosh, Vijay Baiyya, Siddhant Bansal, Bikram Boote, et al. Ego-exo4d: Understanding skilled human activity from first-and third-person perspectives. In *Proceedings of the IEEE/CVF Conference on Computer Vision and Pattern Recognition*, pages 19383–19400, 2024. 3

[14] Shreyas Hampali, Mahdi Rad, Markus Oberweger, and Vincent Lepetit. Honnote: A method for 3d annotation of hand and object poses. In *Proceedings of the IEEE/CVF Conference on Computer Vision and Pattern Recognition (CVPR)*, 2020. 3

[15] Shreyas Hampali, Mahdi Rad, Markus Oberweger, and Vincent Lepetit. Ho-3d\_v3: Improving the accuracy of hand-object poses in the ho-3d dataset. *arXiv preprint arXiv:2107.00887*, 2021. 3, 6, 7

[16] Aaron Hurst, Adam Lerer, Adam P Goucher, Adam Perelman, Aditya Ramesh, Aidan Clark, AJ Ostrow, Akila Welihinda, Alan Hayes, Alec Radford, et al. Gpt-4o system card. *arXiv preprint arXiv:2410.21276*, 2024. 5

[17] Nikita Karaev, Iurii Makarov, Jianyuan Wang, Natalia Neverova, Andrea Vedaldi, and Christian Rupprecht. Co-tracker3: Simpler and better point tracking by pseudo-labelling real videos. *arXiv preprint arXiv:2410.11831*, 2024. 5

[18] Alexander Khazatsky, Karl Pertsch, Suraj Nair, Ashwin Balakrishna, Sudeep Dasari, Siddharth Karamchetti, Soroush Nasiriany, Mohan Kumar Srirama, Lawrence Yunliang Chen, Kirsty Ellis, et al. Droid: A large-scale in-the-wild robot manipulation dataset. *arXiv preprint arXiv:2403.12945*, 2024. 7

[19] Moo Jin Kim, Karl Pertsch, Siddharth Karamchetti, Ted Xiao, Ashwin Balakrishna, Suraj Nair, Rafael Rafailov, Ethan Foster, Grace Lam, Pannag Sanketi, et al. Openvla: An open-source vision-language-action model. *arXiv preprint arXiv:2406.09246*, 2024. 3

[20] Hedvig Kjellstrom, Javier Romero, and Danica Kragic. Visual recognition of grasps for human-to-robot mapping. In *2008 IEEE/RSJ International Conference on Intelligent Robots and Systems*, pages 3192–3199. IEEE, 2008. 3

[21] Hedvig Kjellstrom, Javier Romero, and Danica Kragic. Visual recognition of grasps for human-to-robot mapping. In *2008 IEEE/RSJ International Conference on Intelligent Robots and Systems*, pages 3192–3199. IEEE, 2008. 5

[22] Kailin Li, Puahao Li, Tengyu Liu, Yuyang Li, and Siyuan Huang. Maniptrans: Efficient dexterous bimanual manipulation transfer via residual learning. In *Proceedings of the Computer Vision and Pattern Recognition Conference*, pages 6991–7003, 2025. 4

[23] Kailin Li, Puahao Li, Tengyu Liu, Yuyang Li, and Siyuan Huang. Maniptrans: Efficient dexterous bimanual manipulation transfer via residual learning. In *Proceedings of the Computer Vision and Pattern Recognition Conference*, pages 6991–7003, 2025. 3

[24] Rongao Li, Jie Fu, Bo-Wen Zhang, Tao Huang, Zhihong Sun, Chen Lyu, Guang Liu, Zhi Jin, and Ge Li. Taco: Topics in algorithmic code generation dataset. *arXiv preprint arXiv:2312.14852*, 2023. 6, 7

[25] Bo Liu, Yifeng Zhu, Chongkai Gao, Yihao Feng, Qiang Liu, Yuke Zhu, and Peter Stone. Libero: Benchmarking knowledge transfer for lifelong robot learning. *Advances in Neural Information Processing Systems*, 36:44776–44791, 2023. 7

[26] Songming Liu, Lingxuan Wu, Bangguo Li, Hengkai Tan, Huayu Chen, Zhengyi Wang, Ke Xu, Hang Su, and Jun Zhu. Rdt-1b: a diffusion foundation model for bimanual manipulation. *arXiv preprint arXiv:2410.07864*, 2024. 3

[27] Yao Mu, Tianxing Chen, Shijia Peng, Zanxin Chen, Zeyu Gao, Yude Zou, Lunkai Lin, Zhiqiang Xie, and Ping Luo. Robotwin: Dual-arm robot benchmark with generative digital twins. In *Proceedings of the IEEE/CVF Conference on Computer Vision and Pattern Recognition (CVPR)*, 2025. 3

[28] Georgios Pavlakos, Dandan Shan, Ilija Radosavovic, Angjoo Kanazawa, David Fouhey, and Jitendra Malik. Reconstructing hands in 3d with transformers. In *Proceedings of the IEEE/CVF Conference on Computer Vision and Pattern Recognition*, pages 9826–9836, 2024. 4

[29] Luigi Piccinelli, Christos Sakaridis, Yung-Hsu Yang, Mattia Segu, Siyuan Li, Wim Abbeloos, and Luc Van Gool. Unidepthv2: Universal monocular metric depth estimation made simpler. *arXiv preprint arXiv:2502.20110*, 2025. 4

[30] Aditya Prakash, Matthew Chang, Matthew Jin, and Saurabh Gupta. Learning hand-held object reconstruction from in-the-wild videos. *arXiv preprint*, 2023. 3

[31] Wentian Qu, Zhaopeng Cui, Yinda Zhang, Chenyu Meng, Cuixia Ma, Xiaoming Deng, and Hongan Wang. Novel-view synthesis and pose estimation for hand-object interaction from sparse views. In *Proceedings of the IEEE/CVF international conference on computer vision*, pages 15100–15111, 2023. 3

[32] Balakumar Sundaralingam, Siva Kumar Sastry Hari, Adam Fishman, Caelan Garrett, Karl Van Wyk, Valts Blukis, Alexander Millane, Helen Oleynikova, Ankur Handa, Fabio Ramos, et al. Curobo: Parallelized collision-free robot motion generation. In *2023 IEEE International Conference on Robotics and Automation (ICRA)*, pages 8112–8119. IEEE, 2023. 5

[33] Omid Taheri, Nima Ghorbani, Michael J Black, and Dimitrios Tzionas. Grab: A dataset of whole-body human grasping of objects. In *European conference on computer vision*, pages 581–600. Springer, 2020. 3, 6, 7

[34] Zachary Teed and Jia Deng. Droid-slam: Deep visual slam for monocular, stereo, and rgb-d cameras. *Advances in neural information processing systems*, 34:16558–16569, 2021. 4, 3

[35] Takara E. Truong, Qiayuan Liao, Xiaoyu Huang, Guy Tevet, C. Karen Liu, and Koushil Sreenath. Beyondmimic: From motion tracking to versatile humanoid control via guided diffusion. *arXiv preprint*, 2025. 3

[36] Quan Vuong, Sergey Levine, Homer Rich Walke, Karl Pertsch, Anikait Singh, Ria Doshi, Charles Xu, Jianlan Luo, Liam Tan, Dhruv Shah, et al. Open x-embodiment: Robotic learning datasets and rt-x models. In *Towards Generalist Robots: Learning Paradigms for Scalable Skill Acquisition@ CoRL2023*, 2023. 3

[37] Jikai Wang, Qifan Zhang, Yu-Wei Chao, Bowen Wen, Xiaohu Guo, and Yu Xiang. Ho-cap: A capture system and dataset for 3d reconstruction and pose tracking of hand-object interaction. *arXiv preprint arXiv:2406.06843*, 2024. 3, 6, 7, 8

[38] Ruixiang Wang, Huayi Zhou, Xinyue Yao, Guiliang Liu, and Kui Jia. Gat-grasp: Gesture-driven affordance transfer for task-aware robotic grasping. *arXiv preprint arXiv:2503.06227*, 2025. 3

[39] Bowen Wen, Wei Yang, Jan Kautz, and Stan Birchfield. Foundationpose: Unified 6d pose estimation and tracking of novel objects. In *Proceedings of the IEEE/CVF Conference on Computer Vision and Pattern Recognition*, pages 17868–17879, 2024. 2, 4

[40] Bowen Wen, Matthew Trepte, Joseph Aribido, Jan Kautz, Orazio Gallo, and Stan Birchfield. Foundationstereo: Zero-shot stereo matching. In *Proceedings of the Computer Vision and Pattern Recognition Conference*, pages 5249–5260, 2025. 2, 6

[41] Zhengrong Xue, Shuying Deng, Zhenyang Chen, Yixuan Wang, Zhecheng Yuan, and Huazhe Xu. Demogen: Synthetic demonstration generation for data-efficient visuomotor policy learning. *arXiv preprint arXiv:2502.16932*, 2025. 6

[42] Ge Yan, Kris Wu, and Xiaolong Wang. ucsd kitchens dataset. 2023. 7

[43] Jie Yang, Bingliang Li, Fengyu Yang, Ailing Zeng, Lei Zhang, and Ruimao Zhang. Boosting human-object interaction detection with text-to-image diffusion model. *arXiv preprint arXiv:2305.12252*, 2023. 3

[44] Weirui Ye, Fangchen Liu, Zheng Ding, Yang Gao, Oleh Rybkin, and Pieter Abbeel. Video2policy: Scaling up manipulation tasks in simulation through internet videos. *arXiv preprint arXiv:2502.09886*, 2025. 3

[45] Yufei Ye, Poorvi Hebbar, Abhinav Gupta, and Shubham Tulsiani. Diffusion-guided reconstruction of everyday hand-object interaction clips. In *Proceedings of the IEEE/CVF international conference on computer vision*, pages 19717–19728, 2023. 8

[46] Wanqi Yin, Zhongang Cai, Ruisi Wang, Fanzhou Wang, Chen Wei, Haiyi Mei, Weiye Xiao, Zhitao Yang, Qingping Sun, Atsushi Yamashita, et al. Whac: World-grounded humans and cameras. In *European Conference on Computer Vision*, pages 20–37. Springer, 2024. 2

[47] Jiayao Zhang, Weiyao Huang, Bo Peng, Mingdong Wu, Fei Hu, Zijian Chen, Bo Zhao, and Hao Dong. Omni6dpose: A benchmark and model for universal 6d object pose estimation and tracking. In *European Conference on Computer Vision*, pages 199–216. Springer, 2024. 2

[48] Jinglei Zhang, Jiankang Deng, Chao Ma, and Rolando Alexandros Potamias. Hawor: World-space hand motion reconstruction from egocentric videos. In *Proceedings of the Computer Vision and Pattern Recognition Conference*, pages 1805–1815, 2025. 2

[49] Yuhong Zhang, Jing Lin, Ailing Zeng, Guanlin Wu, Shunlin Lu, Yurong Fu, Yuanhao Cai, Ruimao Zhang, Haoqian Wang, and Lei Zhang. Motion-x++: A large-scale multi-modal 3d whole-body human motion dataset. *arXiv preprint arXiv:2501.05098*, 2025. 3, 4

[50] Yuhong Zhang, Guanlin Wu, Ling-Hao Chen, Zhuokai Zhao, Jing Lin, Xiaoke Jiang, Jiamin Wu, Zhuoheng Li, Hao Frank Yang, Haoqian Wang, et al. Humanmm: Global human motion recovery from multi-shot videos. In *Proceedings of the Computer Vision and Pattern Recognition Conference*, pages 1973–1983, 2025. 2

[51] Tony Z Zhao, Vikash Kumar, Sergey Levine, and Chelsea Finn. Learning fine-grained bimanual manipulation with low-cost hardware. *arXiv preprint arXiv:2304.13705*, 2023. 3, 8

[52] Zibo Zhao, Zeqiang Lai, Qingxiang Lin, Yunfei Zhao, Haolin Liu, Shuhui Yang, Yifei Feng, Mingxin Yang, Sheng Zhang, Xianghui Yang, et al. Hunyuan3d 2.0: Scaling diffusion models for high resolution textured 3d assets generation. *arXiv preprint arXiv:2501.12202*, 2025. 4, 6

[53] Huayi Zhou, Ruixiang Wang, Yunxin Tai, Yueci Deng, Guiliang Liu, and Kui Jia. You only teach once: Learn one-shot bimanual robotic manipulation from video demonstrations. *arXiv preprint arXiv:2501.14208*, 2025. 3

[54] Brianna Zitkovich, Tianhe Yu, Sichun Xu, Peng Xu, Ted Xiao, Fei Xia, Jialin Wu, Paul Wohlhart, Stefan Welker, Ayzaan Wahid, et al. Rt-2: Vision-language-action models transfer web knowledge to robotic control. In *Conference on Robot Learning*, pages 2165–2183. PMLR, 2023. 3

# RoboWheel: A Data Engine from Real-World Human Demonstrations for Cross-Embodiment Robotic Learning

## Supplementary Material

### Contents

<b>A Notations</b>	<b>2</b>
<b>B Transform to Canonical Action Space</b>	<b>3</b>
<b>C Hand Gesture to Robot Arm</b>	<b>4</b>
C.1. Mapping Algorithm	4
C.2. Replay Comparison with Different Methods	4
C.3. Cross-Arm Retargeting Performance	4
<b>D Experiment Details</b>	<b>6</b>
D.1. Implementation and Hyper-Parameters of VLA/IL policies	6
D.2. Training <i>HORA</i> on Maniptrans	6
D.3. Real-world Validation Results	6
<b>E Dataset Details</b>	<b>8</b>
E.1. <i>HORA</i> Mocap Hardware Setup	8
E.2. From Glove Fitting to MANO Parameters	8
E.3. Task Description for <i>HORA</i>	9
<b>F. Data Augmentation</b>	<b>11</b>
F.1. Cross-Embodiment	11
F.2. Background Variation	12
F.3. Object Retrieval	12
F.4. Hand Mirror	12

## A. Notations

Symbol	Meaning	Notes / Space
$\{I_t\}_{t=1}^T$	Input frame sequence	RGB / RGB-D
$K$	Camera intrinsics	Known or estimated
$T_c^w$	Camera pose in world frame	$SE(3)$ ; often $(R_{wc}, t_{wc})$
$\Pi(\cdot)$	Pinhole projection operator	$3D \rightarrow$ pixel coordinates
$\mathbf{h}_t$	Hand state at time $t$	$(\theta_h(t), R_h^w(t), t_h^w(t))$
$\theta_h(t)$	Hand(MANO) parameters	Joint angles
$R_h^w(t), t_h^w(t)$	Wrist pose in world (rot/trans)	$SO(3)$ and $\mathbb{R}^3$
$\mathbf{p}_t$	Object state at time $t$	$T_o^w(t) \in SE(3)$
$T_o^w(t) = (R_o(t), t_o(t))$	Object pose in world (rot/trans)	$SE(3)$
$M_o, \hat{M}_o$	Object mesh (metric / up-to-scale)	Triangle mesh + texture
$s_o$	Object scale factor	From depth–mesh alignment
$m_t, D_t$	Object mask and depth map at $t$	Segmentation and depth
$P_t, P$	Back-projected points (per-frame / global)	From $D_t$ and $K$
AABB( $\cdot$ )	Axis-aligned bounding box	Use diagonal via $\text{diag}(\cdot)$
$\mathbf{A}$	Canonical action space	Unified by C2W and facing origin
$T_w^A = (R^{w \rightarrow A}, t^{w \rightarrow A})$	World-to-action-space transform	Coordinate re-alignment
$\Delta^2(\cdot)$	Second-order temporal difference	Jitter suppression
$\rho(\cdot)$	Robust loss (e.g., Geman–McClure)	For reprojection errors
$d(\cdot, \cdot)$	Point-set / point–surface distance	For proximity/attraction
$V_h, V_o$	Hand mesh vertices / object surface points	Geometry sets
$\phi_h(\mathbf{x}; t)$	Hand signed distance field (SDF)	Positive outside (as used here)
$TSDF_o$	object truncated signed distance function	negative inside and zero else
$\tilde{\mathbf{q}}_i(t)$	World coords of sampled object surface point	$R_o(t) \mathbf{q}_i^{\text{loc}} + t_o(t)$
$\mathcal{N}_t$	Near-contact candidate set	$ \phi_h  < \tau_{\text{band}}$ or Top- $K$
$\ \cdot\ _F$	Frobenius norm	For rotation log etc.
$\log_{SO(3)}(\cdot)$	Lie-group log map on $SO(3)$	Rotation discrepancy
$d_{SE(3)}(\cdot, \cdot)$	Geodesic distance on $SE(3)$	Pose discrepancy
$E_\pi[\cdot]$	Expectation under policy $\pi$	RL objective
$r_t$	Instantaneous reward	Weighted components
$\psi_{\text{limits}}(\cdot)$	Joint-limit margin reward	Prefer mid-range
$\pi_\theta$	Residual policy network	Added to $a^{\text{IK}}$
$T_{\text{rel}}(t)$	Relative pose $T_h^{-1}(t) T_o(t)$	Hand–object relative pose
$R_g, p_g$	Gripper pose (rot/trans)	From hand keypoints
$q_t^{(r)}$	Joint configuration of robot $r$ at $t$	From bounded-rate IK
$\phi_{\text{lim}}(q)$	Joint-limit penalty	IK constraint term
$S = \text{diag}(-1, 1, 1)$	Left–right mirror matrix	About sagittal plane
$R_y(\pi)$	Rotation about $y$ by $\pi$	Used with $S$ to set facing
$\varphi_{\text{sem}}(\cdot)$	Semantic embedding (text–shape)	For semantic similarity
$\gamma^t$	Discount factor power	RL return discounting

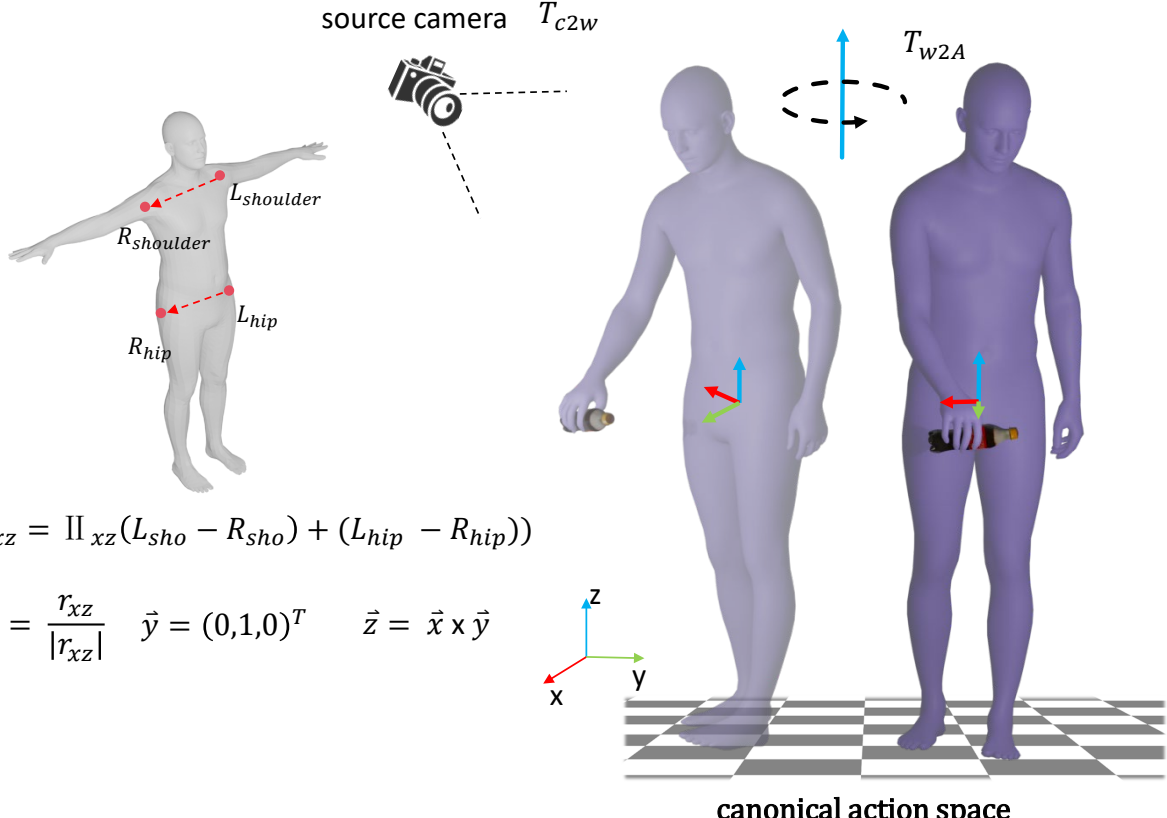


Figure 9. Our pipeline decouples the reconstructed hand-object motions from the specific camera viewpoint of the source video. We first lift the reconstructions to a consistent world frame using the camera-to-world transformation  $T_{c2w}$ . Subsequently, we normalize these trajectories into a canonical action space via  $T_{w2A}$ . This two-step alignment ensures that the retargeted actions maintain a consistent approach direction and kinematic interpretation across all robotic embodiments.

## B. Transform to Canonical Action Space

Real-world HOI videos are captured under arbitrary viewpoints, which leads to view-dependent reconstructions of both hand and object. To eliminate this inconsistency, we adopt a lifting procedure, as shown in Fig. 9. In the first step, all reconstructed HOI results are transformed from their respective camera coordinate systems into the same world coordinate system. In the second step, the trajectories in the world coordinate system are further normalized into a unified canonical action space, ensuring that interaction trajectories from heterogeneous sources become retargetable.

**Step 1: Estimate  $(K, T_c^w)$  and lift to the world frame.** We assume a static-camera prior and estimate camera intrinsics  $K$  and a (time-invariant) camera-to-world transform  $T_c^w = (R_{wc}, t_{wc})$  with DROID-SLAM [34], optimizing sparse/semi-dense reprojection together with temporal smoothness:

$$\begin{aligned} \min_{K, T_c^w} \sum_{t,i} & \left\| \Pi(K, (T_c^w)^{-1}; X_i) - u_{i,t} \right\|_2^2 \\ & + \lambda \left( \|\Delta t_{wc}\|_2^2 + \left\| \log_{SO(3)}(R_{wc}^\top R_{wc}^+) \right\|_2^2 \right), \end{aligned} \quad (6)$$

where  $(\cdot)^+$  denotes the next keyframe. We adopt the keyframe solution as the clipwise  $T_c^w$ . We also evaluated DPVO and COLMAP but found DROID-SLAM more stable on our setting. With the fixed  $T_c^w$  for each clip, we could project our estimated  $\mathbf{h}_t, \mathbf{p}_t$  convert to the world frame:

**Step 2: Align to canonical action space  $\mathcal{A}$ .** Given the left/right hip and shoulder positions  $p_{\text{hip}}^{L/R}, p_{\text{sho}}^{L/R}$  in the world coordinate system  $\{\mathcal{Z}\}$ , we first compute a lateral reference vector on the  $xz$ -plane:

$$v_{\text{lat}} = \Pi_{xz}((p_{\text{hip}}^L - p_{\text{hip}}^R) + (p_{\text{sho}}^L - p_{\text{sho}}^R)).$$

We then construct the canonical frame  $\mathcal{A}$  with the following conventions:

- $z_{\mathcal{A}}$  is aligned with the scene up direction (gravity / ground normal).
- $y_{\mathcal{A}}$  is determined by the dominant interaction direction (e.g., the average hand→object approach vector).
- $x_{\mathcal{A}}$  is obtained by the right-hand rule, ensuring orthonormality.

After orthonormalization, these axes form the rotation matrix  $R_{w \rightarrow \mathcal{A}} \in \text{SO}(3)$ . Finally, we center the action trajectory at the object position (by default, at the first salient frame  $t_0$ ), giving the translation  $t_{w \rightarrow \mathcal{A}} = -R_{w \rightarrow \mathcal{A}} t_o^w(t_0)$  and the resulting rigid transformation  $T_w^{\mathcal{A}} = (R_{w \rightarrow \mathcal{A}}, t_{w \rightarrow \mathcal{A}})$ .

## C. Hand Gesture to Robot Arm

### C.1. Mapping Algorithm

For the two different gesture types, whole-hand and finger-only, we designed corresponding mapping schemes to translate hand motions to a two-fingered gripper. For whole-hand gestures, our method primarily leverages 3d joints on the palm plane to define the gripper’s orientation and spatial position. For finger-only gestures, we incorporate fingertip positions to accommodate dexterous manipulation. The detailed mapping algorithm pseudocode under two gestures is shown in Fig. 10.

---

#### Algorithm 1 Whole-Hand (Palm-Involved) Gripper Pose Construction

---

**Input:** wrist  $\mathbf{k}_{\text{wri}}$ , index MCP  $\mathbf{k}_{\text{ind}}^{\text{mcp}}$ ,  
ring MCP  $\mathbf{k}_{\text{ring}}^{\text{mcp}}$

**Output:** Gripper pose  $(R_g, \mathbf{p}_g)$ .

```

 $\mathbf{w} \leftarrow \mathbf{k}_{\text{wri}}$ ,  $\mathbf{i} \leftarrow \mathbf{k}_{\text{ind}}^{\text{mcp}}$ ,  $\mathbf{r} \leftarrow \mathbf{k}_{\text{ring}}^{\text{mcp}}$ 
    // Extract keypoints
 $\mathbf{o} \leftarrow (\mathbf{w} + \mathbf{i} + \mathbf{r})/3$  // palm origin
 $v_x \leftarrow (\mathbf{r} - \mathbf{w})$  // X-axis direction
 $\bar{\mathbf{x}} \leftarrow v_x/(\text{NORMALIZE}(v_x) + 10^{-8})$ 
    // Normalized X-axis
 $v_z \leftarrow \text{CROSS\_PRODUCT}(\mathbf{i} - \mathbf{w}, \mathbf{r} - \mathbf{w})$ 
    // Z-axis (palm normal)
 $\bar{\mathbf{z}} \leftarrow v_z/(\text{NORMALIZE}(v_z) + 10^{-8})$ 
    // Normalized Z-axis
 $\bar{\mathbf{y}} \leftarrow \text{CROSS\_PRODUCT}(\bar{\mathbf{z}}, \bar{\mathbf{x}})$ 
    // Y-axis direction
 $\bar{\mathbf{z}} \leftarrow \text{SIGN}(\diamond) \cdot \bar{\mathbf{z}}$ 
 $R_g \leftarrow \text{CONCATENATE}([\bar{\mathbf{x}}, \bar{\mathbf{y}}, \bar{\mathbf{z}}])$ 
    // Rotation matrix
 $\mathbf{p}_g \leftarrow \mathbf{o} + d_z \bar{\mathbf{z}}$  // Position
Return  $(R_g, \mathbf{p}_g)$ 

```

---



---

#### Algorithm 2 Finger-Only (Pinch/Precision) Gripper Pose Construction

---

**Input:** index TIP  $\mathbf{k}_{\text{ind}}^{\text{tip}}$ , index MCP  $\mathbf{k}_{\text{index}}^{\text{mcp}}$ , thumb tip  $\mathbf{k}_{\text{thumb}}^{\text{tip}}$ , thumb MCP  $\mathbf{k}_{\text{thumb}}^{\text{mcp}}$

**Output:** Gripper pose  $(R_g, \mathbf{p}_g)$ .

```

 $\mathbf{i} \leftarrow \mathbf{k}_{\text{ind}}^{\text{tip}}$ ,  $\mathbf{m} \leftarrow \mathbf{k}_{\text{ind}}^{\text{mcp}}$ ,  $\mathbf{t} \leftarrow \mathbf{k}_{\text{thumb}}^{\text{tip}}$ ,  $\mathbf{r} \leftarrow \mathbf{k}_{\text{thumb}}^{\text{mcp}}$ 
    // Extract keypoints
 $\mathbf{o} \leftarrow (\mathbf{t} + \mathbf{i})/2$  // palm origin
 $v_z \leftarrow (\mathbf{i} - \mathbf{m})$  // Z-axis direction
 $\bar{\mathbf{z}} \leftarrow v_z/(\text{NORMALIZE}(v_z) + 10^{-8})$ 
    // Normalized Z-axis
 $v_y \leftarrow \text{CROSS\_PRODUCT}(\mathbf{i} - \mathbf{m}, \mathbf{m} - \mathbf{r})$ 
    // Y-axis (palm normal)
 $\bar{\mathbf{y}} \leftarrow v_y/(\text{NORMALIZE}(v_y) + 10^{-8})$ 
    // Normalized Y-axis
 $\bar{\mathbf{x}} \leftarrow \text{CROSS\_PRODUCT}(\bar{\mathbf{y}}, \bar{\mathbf{z}})$ 
    // X-axis direction
 $\bar{\mathbf{z}} \leftarrow \text{SIGN}(\diamond) \cdot \bar{\mathbf{z}}$ 
 $R_g \leftarrow \text{CONCATENATE}([\bar{\mathbf{x}}, \bar{\mathbf{y}}, \bar{\mathbf{z}}])$ 
    // Rotation matrix
 $\mathbf{p}_g \leftarrow \mathbf{o}$  // Position
Return  $(R_g, \mathbf{p}_g)$ 

```

---

Figure 10. Following our gesture classification scheme, we divide grasping into two categories and combine them into the final two-finger gripper pose based on the hand joint space orientation.

### C.2. Replay Comparison with Different Methods

Replay Comparison by Different Methods: We compared the mapping method of *RoboWheel* with YOTO and GAT-Grasp. YOTO and GAT-Grasp result in discrepancies in gripper position or orientation mapping, leading to failure, while *RoboWheel* provides more accurate and reasonable mapping, as shown in Fig. 11.

### C.3. Cross-Arm Retargeting Performance

In Tab. 5, we report the real-world SR of different mapping methods on UR5. To further assess the generalization and scalability of our approach, we deploy the same mapping algorithm across multiple manipulators (UR5, Gen3, iiwa7, Sawyer, and Franka) in simulation. As shown in Tab. 6, our method achieves consistently high performance on all arms, with SR

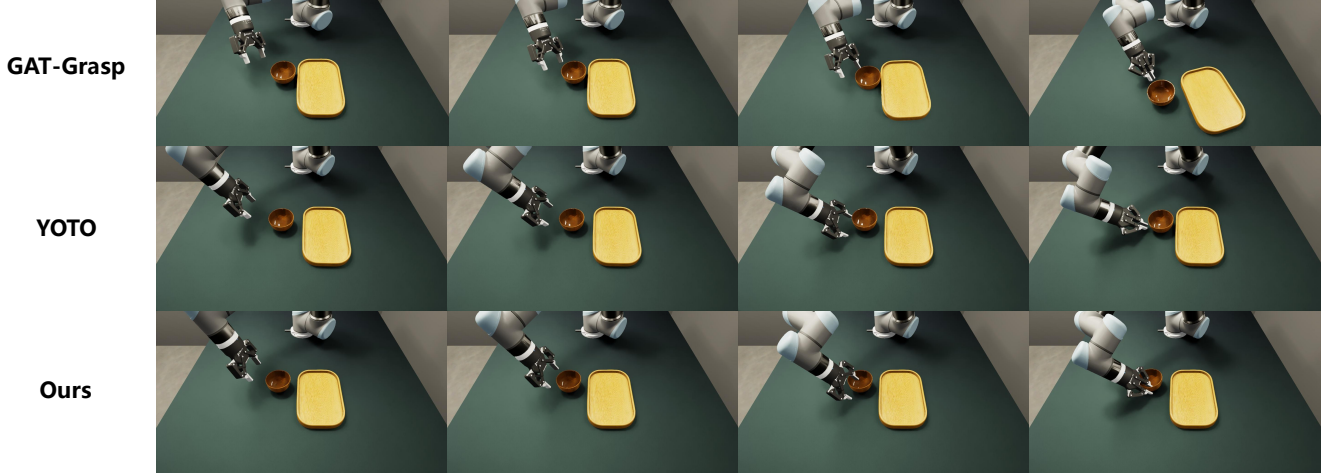


Figure 11. Replay Comparison by Different Methods: We compared the mapping method of *RoboWheel* with YOTO and GAT-Grasp. YOTO and GAT-Grasp result in discrepancies in gripper position or orientation mapping, leading to failure, while *RoboWheel* provides more accurate and reasonable mapping.

<b>Task</b>	<b>UR5</b>	<b>Gen3</b>	<b>iiwa7</b>	<b>Sawyer</b>	<b>Franka</b>
flip_milk	10/10 (100%)	10/10 (100%)	7/10 (70%)	10/10 (100%)	7/10 (70%)
place_milk	10/10 (100%)	10/10 (100%)	10/10 (100%)	10/10 (100%)	10/10 (100%)
pour_cola	10/10 (100%)	10/10 (100%)	10/10 (100%)	10/10 (100%)	10/10 (100%)

Table 6. Scaled success rates for 10 trials per task using the same retarget method.

remaining stable despite differences in kinematics and embodiments. This indicates that the proposed mapping is robust and scalable for cross-embodiment transfer.

## D. Experiment Details

We used the *HORA* to train four VLA/IL policies, namely ACT, DP, RDT-1B, and Pi0, to validate the effectiveness of our data. Before training these models, we preprocessed the data into the format of observations, actions, and instructions (if required) for model training.

### D.1. Implementation and Hyper-Parameters of VLA/IL policies

For ACT, we trained each task for 20,000 iterations, with 90% of the data used for training and the remaining 10% for validation. When training DP, we kept the same training steps, learning rate, and chunk size as ACT. The specific hyperparameter values are listed in Tab. 7.

ACT		DP	
Hyperparameter	Value	Hyperparameter	Value
Chunk size	16	Chunk size	16
Hidden dim	512	Action horizon	8
Batch size	16	Batch size	16
Learning rate	1e-5	Learning rate	1e-5
Dim feedforward	3200	Observation horizon	8
Training steps	20000	Training steps	20000

Table 7. Hyperparameters used to train ACT and DP.

**RDT** was pretrained for 100,000 steps with a batch size of 8 per GPU on 4 GPUs, and all single-task fine-tuning was conducted for 10,000 steps with a batch size of 8 per GPU on a single GPU. **Pi0** was pretrained for 100,000 steps with a batch size of 32 on 8 GPUs, and all fine-tuning was performed for 30,000 steps using the same batch size on a single GPU.

All remaining hyperparameters for RDT and Pi0 were set according to their official documentation.

### D.2. Training *HORA* on Maniptrans

We mapped the hand gestures onto the dexterous hands and completed the training in a simulation environment. The training outcomes are shown in Fig. 12.

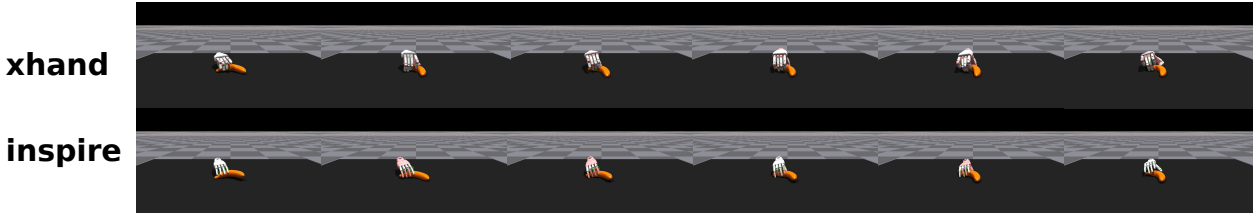


Figure 12. Visualization results of maniptrans

### D.3. Real-world Validation Results

Here, we present the experimental results for all designed tasks conducted on physical robot(UR5),as shown in Fig. 13.



Figure 13. Visualization of eight tasks on real robot

## E. Dataset Details

We construct a large-scale dataset (*HORA*) with three subsets: *HORA-Mocap* (multi-view mocap with tactile gloves), *HORA-Recordings* (in-house RGB(D) recordings without tactile), and *HORA-Public* (retargeted public HOI datasets).

### E.1. *HORA* Mocap Hardware Setup

**Glove** The glove is instrumented with 16 Gen3 tactile sensors and 29 magnetic encoders. Worn on a single hand, it enables the acquisition of high-frequency tactile data. The tactile sensors are capable of detecting pressure, force, and vibration, while the magnetic encoders are used to capture precise joint angles and movements of the fingers. This combination allows for detailed hand-object interaction data to be gathered with high temporal resolution. Visualization of the Mocap Hardware setup and gloves in simulation is shown as Fig. 14.



Figure 14. Visualization of the Mocap Hardware setup and gloves in simulation.

**RGBD Cameras** Three Intel RealSense D455 RGBD cameras are used to capture depth and RGB data simultaneously. The cameras are mounted at strategic locations to ensure optimal coverage and accurate 3D spatial data. The depth cameras provide high-resolution depth maps, while the RGB cameras offer high-quality color images. For synchronized data acquisition, a synchronization cable is employed, connecting three cameras to ensure precise temporal alignment across all devices.

**RGB Cameras** A total of eight high-resolution RGB cameras are used for detailed visual tracking. These cameras are positioned to cover different angles, enabling comprehensive capture of the environment and subjects. The cameras are used to provide complementary visual data to the depth information provided by the RGBD cameras.

### E.2. From Glove Fitting to MANO Parameters

We retarget glove-based kinematic fits to the MANO hand model through a unified differentiable optimization. Both the glove and MANO use differentiable forward kinematics (FK), allowing a smooth transition that preserves global pose and local contact geometry.

**Glove-domain fitting.** We first calibrate the glove using multi-view constraints. To ensure consistent correspondence, we define: (i) a link-level mapping between glove joints and MANO joints, and (ii) tactile sensor points assigned to glove links. Contact constraints are activated only for links with nonzero force. If a link has no force, its position/normal constraints are disabled. For links under force, we apply force-aware weights: strong-force sensor points have weight 1.0, while other activated points have weight 0.3. The glove fitting objective is

$$\mathcal{L}_{\text{glove}} = \mathcal{L}_{\text{contact}} + \mathcal{L}_{\text{wrist}} + \mathcal{L}_{\text{jlim}} + \mathcal{L}_{\text{smooth}} + \mathcal{L}_{\text{anat}}, \quad (7)$$

where  $\mathcal{L}_{\text{contact}}$  aligns positions and normals at tactile points,  $\mathcal{L}_{\text{wrist}}$  constrains the wrist pose,  $\mathcal{L}_{\text{jlim}}$  penalizes joint-limit violations,  $\mathcal{L}_{\text{smooth}}$  enforces temporal smoothness, and  $\mathcal{L}_{\text{anat}}$  regularizes anatomical plausibility. All frames are optimized in parallel. To handle wrist floating, we prepend a free 6-DoF transform before the glove wrist base.

**Retargeting initialization.** The optimized glove motion is used to initialize MANO. We copy the glove global wrist transform (including the 6-DoF floating pose) to MANO’s root pose, and map each glove joint rotation to its corresponding MANO joint using the predefined correspondence. This yields an initial MANO pose close to the contact-consistent glove fit.

**MANO refinement.** Starting from the retargeted initialization, we refine MANO parameters under the same constraints, now expressed on MANO joints/vertices. MANO pose is parameterized by 16 articulated joints, each with 3-DoF axis-angle rotations, i.e.,

$$\boldsymbol{\theta} \in \mathbb{R}^{16 \times 3}, \quad (8)$$

together with a global wrist pose. We minimize

$$\mathcal{L}_{\text{mano}} = \mathcal{L}_{\text{contact}} + \mathcal{L}_{\text{wrist}} + \mathcal{L}_{\text{jlim}} + \mathcal{L}_{\text{smooth}} + \mathcal{L}_{\text{anat}}, \quad (9)$$

using the same force-aware contact weights transferred from glove links. This refinement produces anatomically valid MANO poses while preserving tactile interaction geometry.

### E.3. Task Description for *HORA*

The *HORA*-Mocap subset is designed to provide a compact yet diverse set of everyday household manipulation skills captured with high-fidelity motion tracking. We curate tasks that range from simple, atomic primitives (e.g., pick-and-place, pressing, pouring, inserting, and opening/closing) to mid- and long-horizon activities that require multi-step coordination and object-centric reasoning (e.g., pouring water into a cup, storing blocks, tabletop cleaning, tong-based picking, and bulb installation). To reflect realistic human hand usage, the task taxonomy is simplified into one-handed and two-handed categories, covering both single-handed interactions and cooperative bimanual behaviors such as rotating a cap, folding clothes, scanning items, and table setting. For detailed task descriptions and visualization, please refer to the Tab.8 and Fig.15. The resulting task suite offers a structured benchmark for learning and evaluating dexterous manipulation policies under varied object types, action primitives, and temporal horizons.

#	Task type	Primitive / skill	Manipulated objects	Task description
1	One-handed	pick&place	Coconut water bottle (350 ml)	Pick up and place the object.
2	One-handed	pick&place	Black marker	Pick up and place the object.
3	One-handed	pick&place	Lidded ceramic mug (white)	Pick up and place the object.
4	One-handed	pick&place	Claw hammer	Pick up and place the object.
5	One-handed	press	Remote control	Press buttons on the remote control.
6	One-handed	pour	Kettle	Pick up the kettle and perform a pouring motion.
7	One-handed	insert	Gel pen + pen holder	Insert the pen into the pen holder.
8	One-handed	open-close	Tea gift box	Open the tea gift box and then close it.
9	One-handed	pouring water	Kettle + cup	Place the cup at a fixed position, pick up the kettle to pour water, put down the kettle, then deliver the cup to a target position.
10	One-handed	block storage	Blocks + block box	Store blocks of different shapes into the block box.
11	One-handed	tabletop wiping	Cleaning sponge	Hold the sponge and wipe the tabletop.
12	One-handed	vacuum cleaning	Handheld vacuum	Use the handheld vacuum to clean the tabletop.
13	One-handed	tong picking	Baking tongs + bun-shaped object	Use tongs to pick up the bun-shaped object.
14	One-handed	bulb installation	Light bulb + bulb socket	Screw the light bulb into the socket.
15	Two-handed	pick&place	Large plate	Pick up and place the object with both hands.
16	Two-handed	pick&place	Large juice bottle	Pick up and place the object with both hands.
17	Two-handed	rotate	Bottle with cap	Cooperatively unscrew the cap with both hands, then re-tighten it.
18	Two-handed	clothes folding	T-shirt	Fold the T-shirt and place it at a fixed position.
19	Two-handed	item scanning	Scanner gun + items to scan	Pick up an item and scan it with the scanner gun.
20	Two-handed	table setting	Tableware set	Set the table following Western-style table-setting rules.

Table 8. *HORA*-Mocap subset task list.

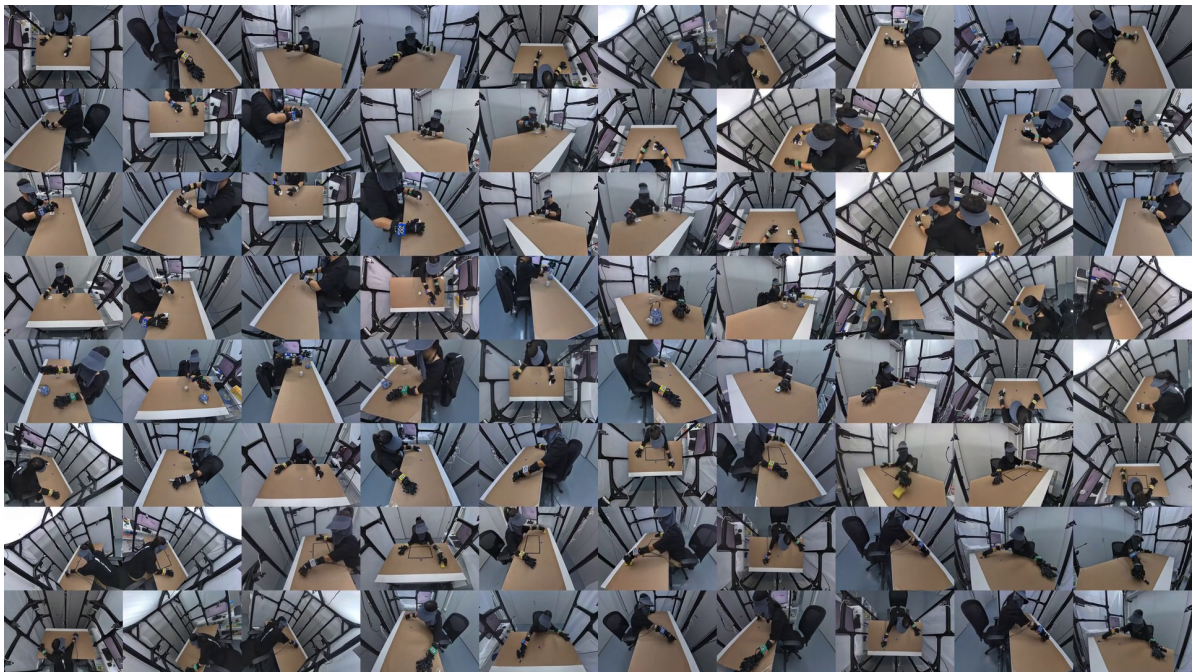


Figure 15. *HORA*-Mocap Overview,

## F. Data Augmentation

In this section, we present various data augmentation strategies and additional details applied to more tasks.

### F.1. Cross-Embodiment

Here, we present additional results from the data augmentation module, demonstrating motion retargeting for HOI reconstruction to different robotic arms. Fig. 16 and Fig. 17 show the retargeted motions for the tasks "flip milk," "pour water," and "place milk" to the *UR5/UR5e*, *Franka Emika Panda*, *KUKA LBR iiwa 7*, *Kinova Gen3*, and *Rethink Robotics Sawyer* arms, respectively.

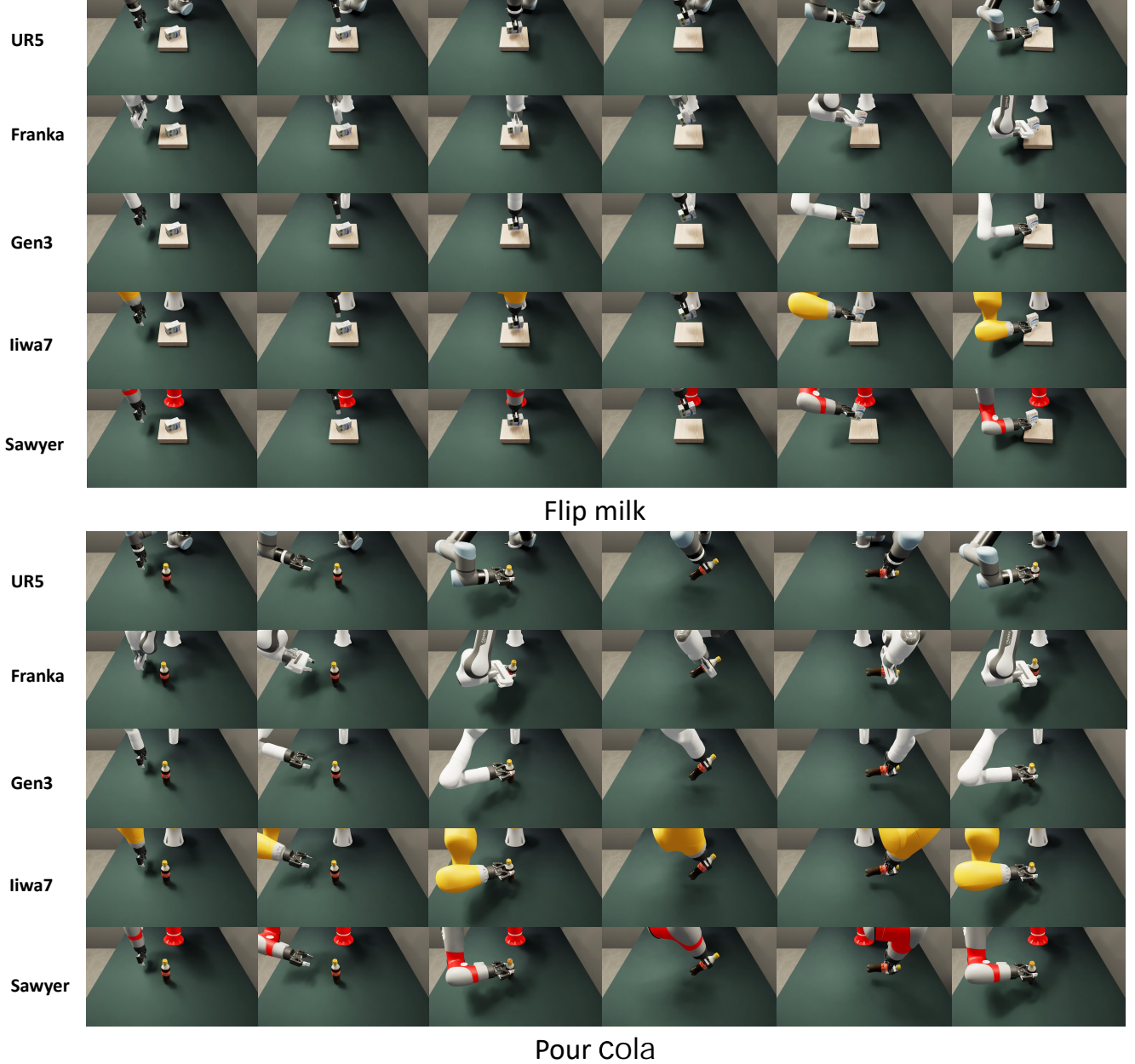


Figure 16. Visualization of robot arm augmentation: flip milk and pour Water

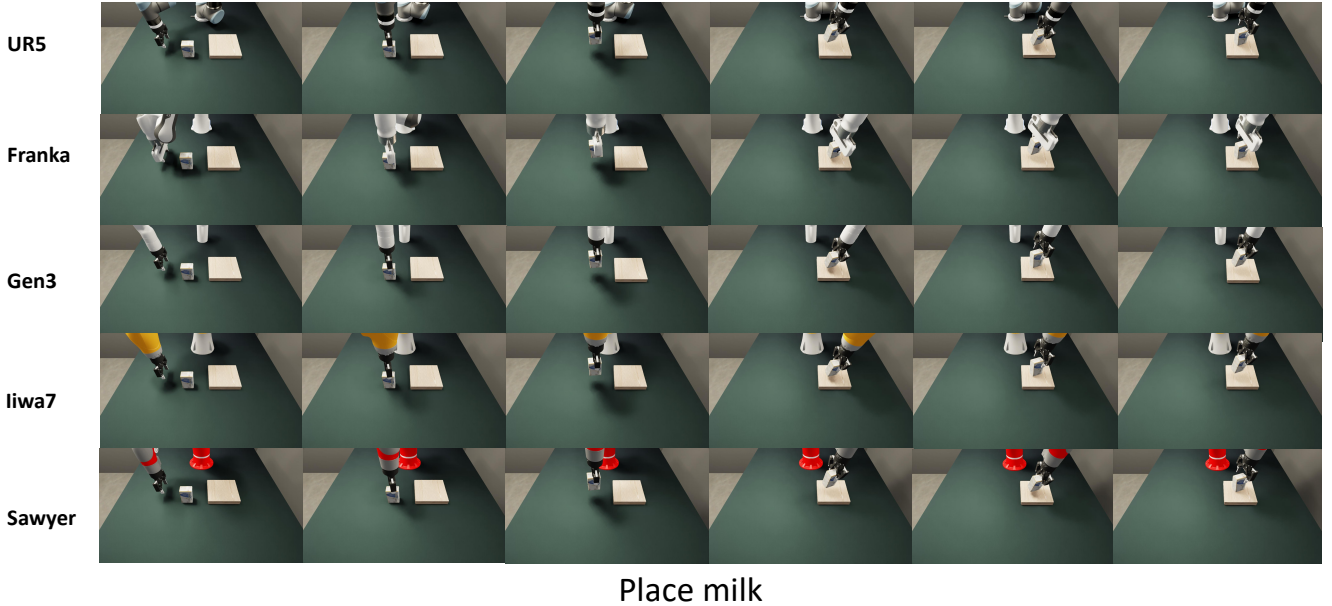


Figure 17. Visualization of robot arm augmentation:place milk

## F.2. Background Variation

As shown in Fig. 18, we apply scene-level visual randomization to diversify the pixel distribution while keeping task dynamics and contact semantics unchanged: *i*) workspace and background appearance randomization (e.g., tabletop, backsplash) via texture and normal-map swaps, and adjustment of basic PBR parameters (albedo/roughness); *ii*) illumination randomized using parametric light sources with variations in spatial placement, intensity, color, color temperature, and emission radius, enabling a broad range of plausible lighting conditions; *iii*) clutter regime ranging from empty scenes to heavy distractors, with randomly sampled object positions and orientations placed collision-free outside the robot’s swept volume via rejection sampling; *iv*) mild camera intrinsics/extrinsics jitter consistent with prior calibration to emulate plausible view changes.

## F.3. Object Retrieval

Our object-retrieval augmentation strategy successfully enables the transfer of manipulation skills to novel objects in simulation. By replacing the original object with a retrieved counterpart that shares high geometric and semantic similarity, and initializing it in the same canonical pose, the robot can reliably execute the same action trajectory. Visually confirmed in Fig. 19, Fig. 20, and Fig. 21 for tasks including “pour water”, “tip tea cup”, and “place box”.

## F.4. Hand Mirror

**Motivation.** Many daily manipulations are left-right symmetric up to a sagittal-plane reflection; mirroring increases trajectory diversity without changing task semantics.

**Operator.** Let the sagittal reflection be  $S = \text{diag}(-1, 1, 1)$ . For positions,  $p'(t) = S p(t)$ . A pure reflection is improper for orientations, so we compose a  $\pi$ -rotation about the  $y$ -axis to recover a proper rotation:

$$R'(t) = S R(t) S \cdot R_y(\pi), \quad \det(R'(t)) = +1. \quad (10)$$

We mirror *both* hand and object about the same plane so that  $T'_{\text{rel}}(t) = T'_h(t)^{-1} T'_o(t) = T_{\text{rel}}(t)$ , preserving contact frames and approach vectors. Gripper chirality and finger-axis signs are flipped consistently.

**Safeguards.** We exclude actions whose handedness encodes semantics (e.g., threaded fasteners), detected via a non-zero screw component about the task  $z$ -axis exceeding  $\tau_{\text{screw}}$ . Mirrored rollouts must pass the replay check on a reference arm before inclusion.

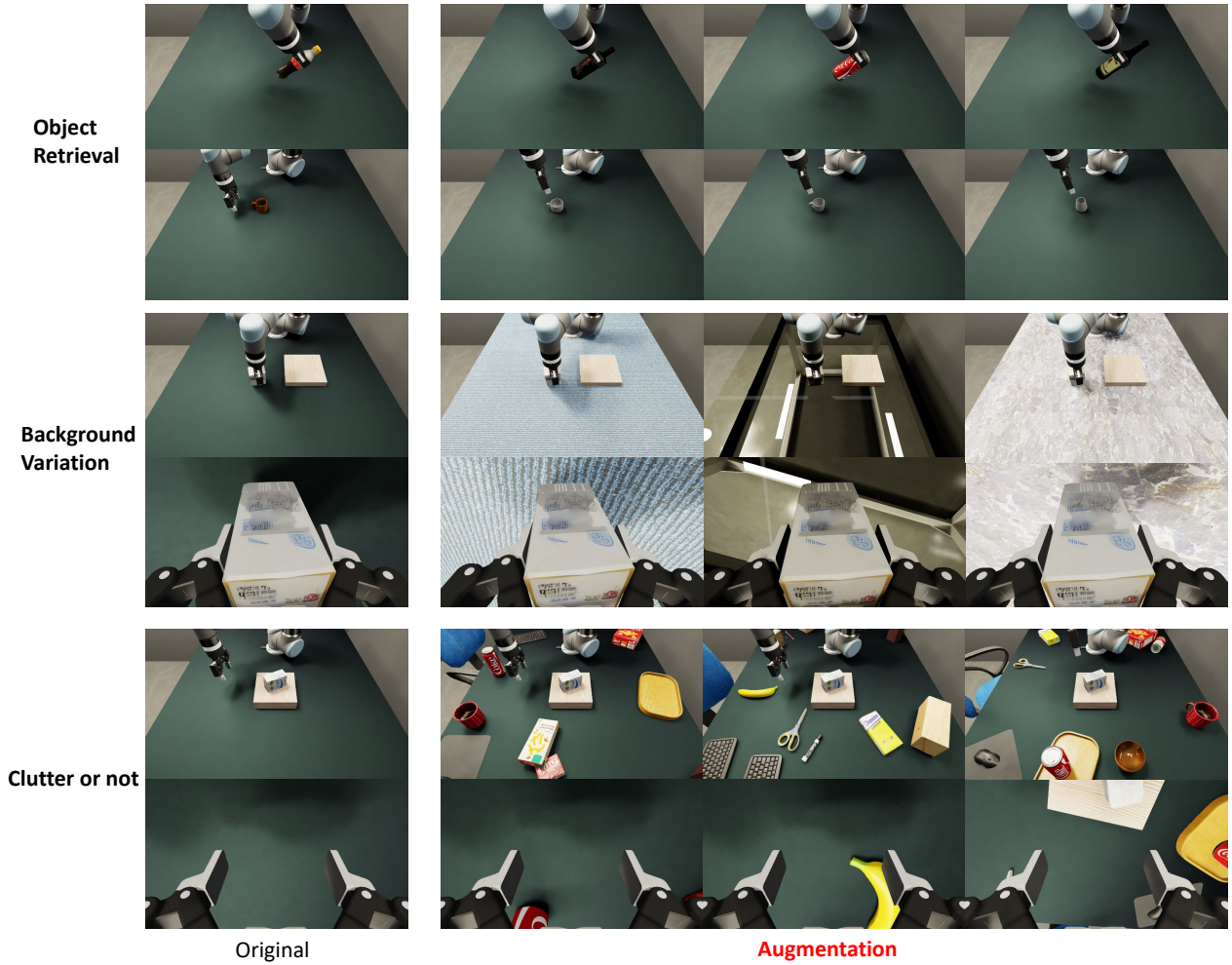


Figure 18. Diverse background texture augmentation in *RoboWheel*.

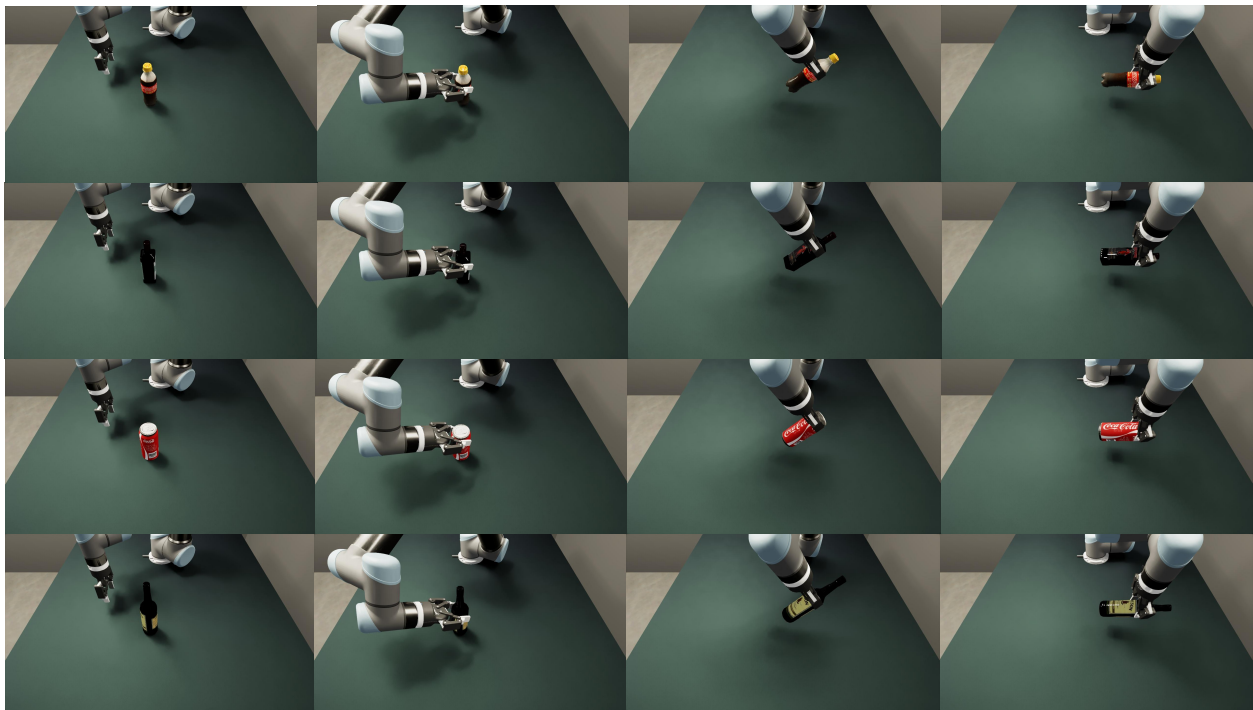


Figure 19. Object Retrieval augmentation

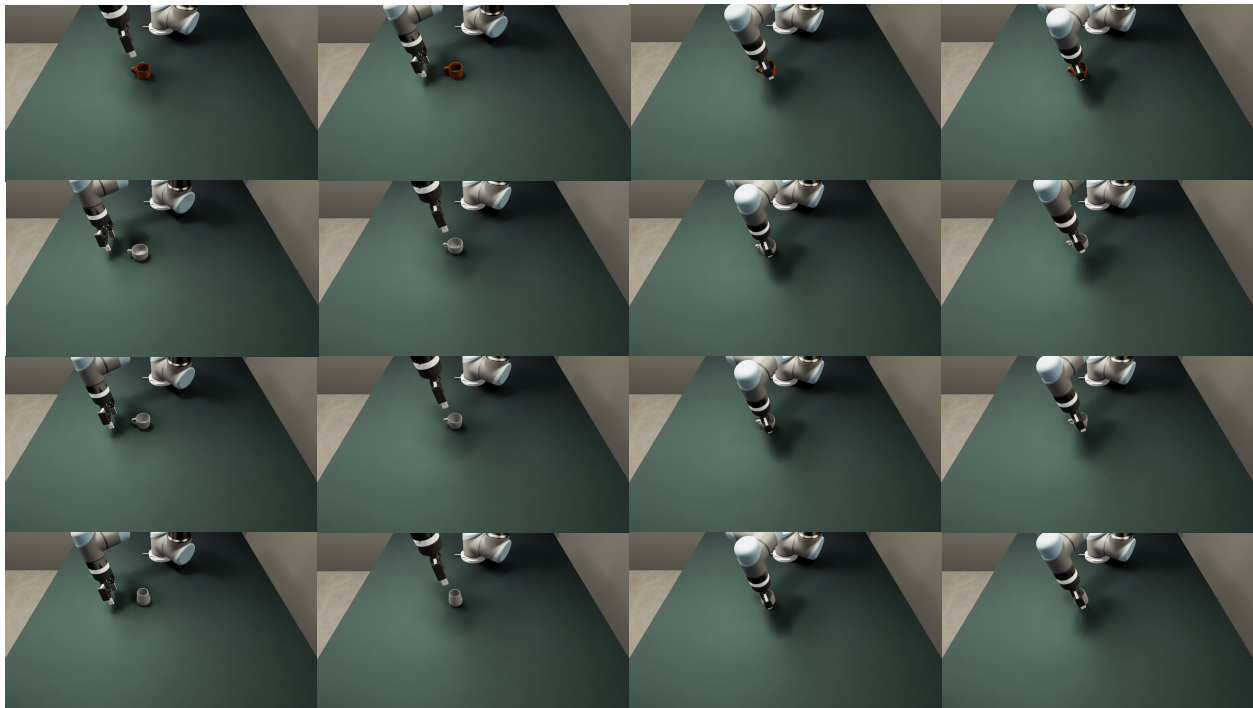


Figure 20. Object Retrieval augmentation

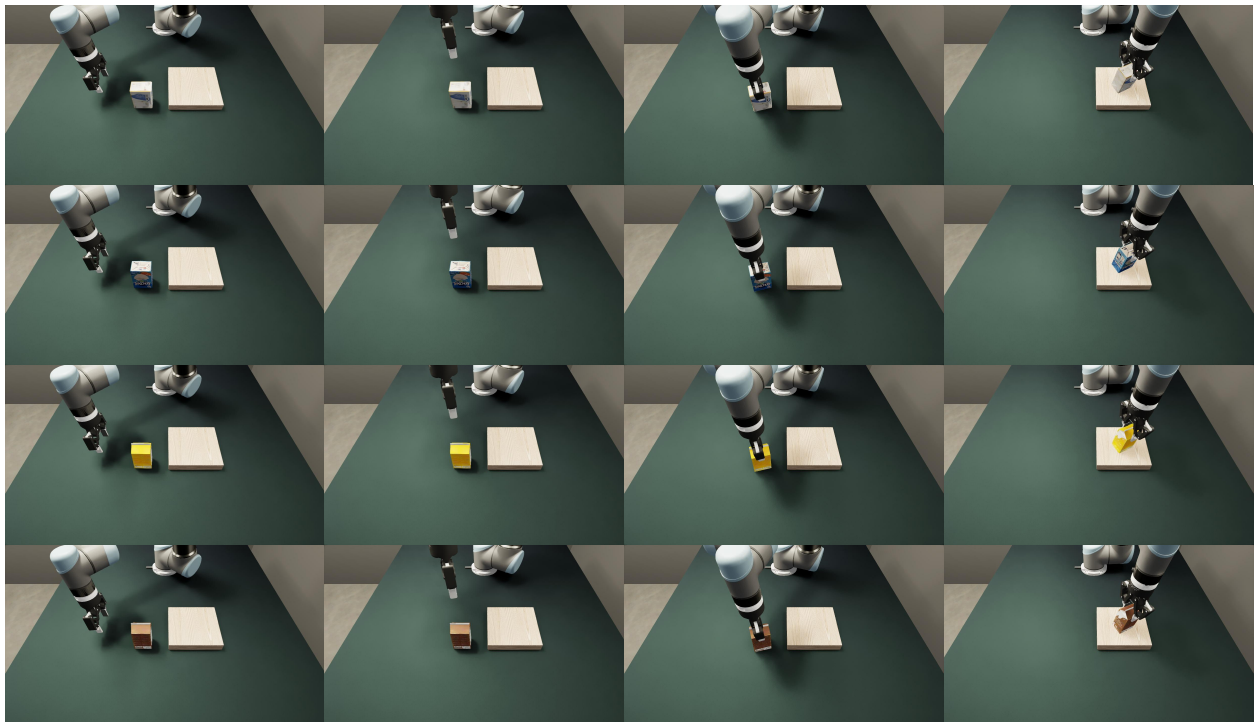


Figure 21. Object Retrieval augmentation